NEUROSCIENCE

Stepwise synaptic plasticity events drive the early phase of memory consolidation

Akihiro Goto[1,2], Ayaka Bota[1,2,3], Ken Miya[2,4,5], Jingbo Wang[1], Suzune Tsukamoto[1], Xinzhi Jiang[1], Daichi Hirai[2], Masanori Murayama[2,6], Tomoki Matsuda[7], Thomas J. McHugh[2,6], Takeharu Nagai[7], Yasunori Hayashi[1,2,8]*

Memories are initially encoded in the hippocampus but subsequently consolidated to the cortex. Although synaptic plasticity is key to these processes, its precise spatiotemporal profile remains poorly understood. Using optogenetics to selectively erase long-term potentiation (LTP) within a defined temporal window, we found that distinct phases of synaptic plasticity play differential roles. The first wave acts locally in the hippocampus to confer context specificity. The second wave, during sleep on the same day, organizes these neurons into synchronously firing assemblies. Finally, LTP in the anterior cingulate cortex during sleep on the second day is required for further stabilization of the memory. This demonstrates the precise localization, timing, and characteristic contributions of the plasticity events that underlie the early phase of memory consolidation.

The current prevailing view of episodic memory is that it is initially encoded in the hippocampus and subsequently transferred to other regions, including the cerebral cortex, for long-term storage in a process termed memory consolidation (*1*, *2*). It has been proposed that synaptic plasticity may underlie learning, which is assumed to play a critical role in memory consolidation (*3*, *4*). However, it remains largely unknown where and when synaptic plasticity occurs, along with the more complex question of how synaptic plasticity shapes neuronal representation. This is due primarily to a lack of appropriate experimental techniques to detect and modify synaptic plasticity in a precise spatiotemporal manner. We thus developed an optogenetic method to selectively erase long-term potentiation (LTP) without affecting basal transmission or precluding future plasticity events.

Optical erasure of sLTP

Previous studies have demonstrated that the early phase of LTP is associated with rapid polymerization of actin within dendritic spines, which acts to enlarge their structure [structural LTP (sLTP)](*5*). At the same time, cofilin (CFL), an F-actin side-binding protein, accumulates at the bottom of the spine head (*6*). CFL exerts differential effects on F-actin depending on its density on the filament (*7*, *8*). At low density, CFL twists and severs F-actin, leading to its disassembly. By contrast, when CFL binds F-actin at a high stoichiometric ratio, it forms cofilactin, thus stabilizing F-actin. We previously demonstrated that sLTP induction promotes CFL-actin interaction, consistent with the formation of cofilactin (*6*). Therefore, we hypothesized that inactivating CFL would lead to destabilization of the cofilactin structure within the dendritic spine, thereby permitting selective erasure of sLTP.

To test this, we employed the genetically encoded photosensitizer protein SuperNova (SN), which allows for chromophore-assisted light inactivation (CALI) of specific molecules in living cells. Upon illumination at specific wavelengths, SN generates reactive oxygen species that inactivate the proteins to which it is fused (*9*, *10*). In nonneuronal cells expressing a fusion protein of CFL with SN (CFL-SN), induction of CALI by light illumination inhibited the actin-dependent motility of lamellipodia, consistent with the inactivation of CFL (fig. S1) (*9*, *11*). We then coexpressed CFL-SN with CFL–green fluorescent protein (GFP) in CA1 pyramidal neurons in hippocampal slice cultures, together with DsRed2 as a volume filler. Owing to the cooperativity of CFL binding to F-actin, we predicted that CALI of CFL-SN would also lead to dissociation of CFL-GFP from F-actin. Upon induction of sLTP by two-photon uncaging of MNI (4-methoxy-7-nitroindolinyl)-glutamate at single dendritic spines, we observed a rapid accumulation of CFL-GFP, overshooting the increase in volume (*6*) (Fig. 1, A and B). By inducing CALI 10 min after sLTP induction, both the enrichment of CFL-GFP and the increase in spine volume were reversed.

sLTP is accompanied by decreased actin turnover within dendritic spines (*12*). To establish whether the enriched CFL and resulting cofilactin formation are involved in this process, we tested whether CALI of CFL-SN can restore actin turnover using photoactivatable GFP (PAGFP)–fused actin (*12*). Photoactivation of PAGFP-actin at the tip of dendritic spines revealed actin turnover within the body of the dendritic spine, which slowed after the induction of sLTP (Fig. 1C). However, when CALI was performed after sLTP induction, actin turnover was restored and spine volumes returned to baseline levels. Overall, these results are consistent with the idea that cofilactin structure maintains the increase in spine volume after sLTP induction, and that CALI of CFL-SN can efficiently reverse sLTP by destabilizing this structure and restoring actin turnover (fig. S2).

Time window of optical erasure of sLTP

To understand the temporal window of effectiveness, CALI was triggered at multiple time points after sLTP induction. Light illumination of spines expressing CFL-SN 10 min after LTP led to a decrease in spine enlargement compared with spines expressing an unfused SN (Fig. 1, D and E). Similarly, 30 min after sLTP induction, CALI remained effective in reducing spine volume. However, this effect was not evident after 50 min (Fig. 1F) (*6*). CALI applied to spines 1 min before sLTP had no effect on its subsequent expression (Fig. 1F). Moreover, CALI triggered in spines where sLTP had not been induced had no effect on spine volume regardless of its original size (Fig. 1, D and E, and fig. S3). Reinduction of sLTP in the same spine after CALI was still possible, indicating that the procedure does not cause permanent damage, but only temporarily disrupts the spine-associated plasticity machinery (Fig. 1E and fig. S4).

Electrically recorded LTP can also be optically erased

To test whether CALI of CFL-SN could erase electrically recorded LTP, field excitatory postsynaptic potentials (fEPSPs) were recorded in the CA1 stratum radiatum of hippocampal slices from CaMKIIα-Cre mice infected with AAV_2-EF1α-DIO-CFL-SN (fig. S5A). LTP was induced by high-frequency stimulation (HFS) and CALI was triggered 10 min later. fEPSPs were specifically decreased in the LTP pathway, but not in the control pathway or in slices expressing unfused SN (fig. S5B). Subsequent HFS produced a sustained potentiation of the fEPSPs, indicating that CALI selectively erased the existing LTP without interfering with any future plasticity events. When CALI was conducted either 1 min before or 50 min after LTP induction, it did not have any impact on potentiation (fig. S5, B and C). Because both *N*-methyl-d-aspartate receptor- and metabotropic glutamate receptor-dependent long–term depression (LTD) share CFL as a

[1]Department of Pharmacology, Kyoto University Graduate School of Medicine, Kyoto 606-8501, Japan. [2]RIKEN Brain Science Institute, Wako, Saitama 351-0198, Japan. [3]Graduate School of Science and Engineering, Saitama University, Saitama 338-8570, Japan. [4]Department of Molecular Neurobiology, Faculty of Medicine, University of Tsukuba, Tsukuba, Ibaraki 305-8575, Japan. [5]Graduate School of Comprehensive Human Sciences, University of Tsukuba, Tsukuba, Ibaraki 305-8575, Japan. [6]RIKEN Center for Brain Science, Wako, Saitama 351-0198, Japan. [7]SANKEN (The Institute of Scientific and Industrial Research), Osaka University, Mihogaoka 8-1, Ibaraki, Osaka 567-0047, Japan. [8]Brain and Body System Science Institute, Saitama University, Saitama 338-8570, Japan.
*Corresponding author. Email: yhayashi-tky@umin.ac.jp

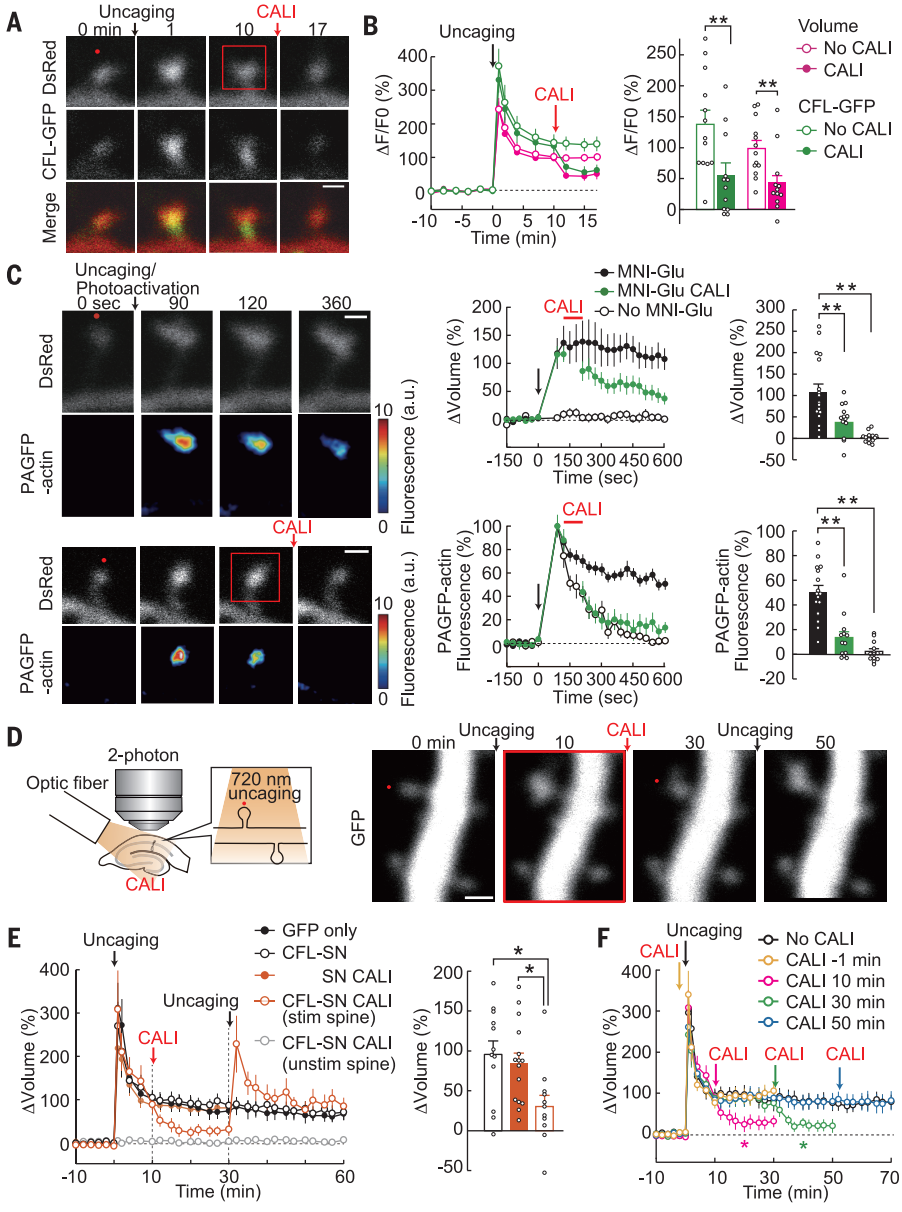

Fig. 1. Optical erasure of sLTP. (**A**) DsRed2 (top) and CFL-GFP (bottom) images. Persistent enlargement of the spine was induced with two-photon (2P) uncaging of MNI-glutamate in single dendritic spines in hippocampal slice cultures, which expressed CFL-SN, CFL-GFP, and DsRed2. The red dot in the DsRed2 image indicates the uncaging spot. A 559-nm laser was irradiated within the square region to induce CALI in the stimulated spine. Scale bar, 1 μm. (**B**) Time courses of changes in spine volume and the amount of CFL-GFP relative to the averaged baseline fluorescence intensity from spines without illumination (n = 13) and spines with 593-nm illumination 10 min after sLTP induction (n = 12) (left). Summary of changes in the intensity of CFL-GFP and spine volume 5 min after CALI (right). Wilcoxon signed-rank test, P = 0.0098 (volume), P = 0.0043 (CFL-GFP). (**C**) Images of DsRed2 and PAGFP-actin in spines. Red dots in the DsRed2 images indicate uncaging and photoactivation points. 559-nm light was illuminated within the square region around the spine head. The fluorescence of PAGFP after photoactivation was normalized to 100%. With MNI-glutamate without CALI (n = 15), with MNI-glutamate and CALI (n = 14), without MNI-glutamate and CALI (n = 13). Averaged spine volume 600 s after uncaging and photoactivation are shown as bar graphs. One-way analysis of variance (ANOVA) test followed by Tukey-Kramer post hoc test (versus MNI-Glu). ΔVolume; P = 0.0027 (MNI-Glu CALI), P = 0 (No MNI-Glu), $F_{2,41}$ = 15.05. Fluorescence; P = 0.0001 (MNI-Glu CALI), P = 0 (No MNI-Glu), $F_{2,41}$ = 17.72. Scale bars, 1 μm. a.u., arbitrary units. (**D**) Field illumination of neurons expressing CFL-SN and GFP in hippocampal slice cultures (left). To induce CALI, a 593-nm laser (0.8W/cm^2, 60 sec, 2-mm diameter spot) was illuminated using an optic fiber. GFP images of a representative neuron expressing CFL-SN and GFP (right). Red dots indicate two-photon uncaging spots. A 593-nm laser was irradiated 10 min after LTP induction. Scale bar, 1 μm. (**E**) Summary of effect of CALI of CFL-SN on sLTP. Spine volume was quantified by measuring the total GFP fluorescence intensity relative to the baseline intensity. Neurons expressing GFP only without CALI (GFP only, n = 12), CFL-SN and GFP without CALI (CFL-SN No CALI, n = 12), SN and GFP with CALI (SN CALI, n = 15), CFL-SN and GFP with CALI (CFL-SN CALI, both glutamate stimulated and unstimulated adjacent spines, n = 12). Averaged spine volume 7 min after CALI are shown as bar graphs. One-way ANOVA test followed by Tukey-Kramer post hoc test. P = 0.0119 (CFL-SN versus CFL-SN CALI), P = 0.0335 (SN CALI versus CFL-SN CALI), $F_{2,36}$ = 5.34. (**F**) Effect of CALI of CFL-SN on sLTP at various time points before and after induction. CALI was conducted 1 min before sLTP induction or 10, 30, and 50 min after induction. Wilcoxon signed-rank test, 10 min after CALI of each CALI group versus control (No CALI), P = 0.1811 (CALI 1 min, n = 12), P = 0.0221 (CALI 10 min, n = 12), P = 0.0306 (CALI 30 min, n = 10), P = 0.9732 (CALI 50 min, n = 13). Means ± SEMs are shown; significance is indicated in the figures as follows: *: P < 0.05; **: P < 0.01.

common downstream mediator (*13*, *14*), it was necessary to characterize the effects of CALI on LTD. However, we observed no effect on low-frequency stimulation–induced LTD (fig. S5D).

Optical erasure of LTP impairs context-specific memory within a specific time window

Next, we tested whether we could erase memories in intact animals. CFL-SN was expressed bilaterally in dorsal CA1 of the hippocampus by injecting AAV$_2$-EF1α-DIO-CFL-SN in CaMKIIα-Cre mice, and optic fibers were implanted above the area of injection (Fig. 2A). Memory was assessed using an inhibitory avoidance (IA) learning paradigm. In this task, mice were placed in the lit side of a partitioned chamber. They typically crossed over to the dark side within 30 s of the door opening, where they received a foot shock (Fig. 2B). Although naïve animals (no virus injection or illumination) showed a prolonged crossover latency to the dark side on day 2, mice expressing CFL-SN that underwent CALI 2 min after the shock had significantly shorter latencies, indicating that memory formation was disrupted (Fig. 2C). The same mice were able to form the memory after they were shocked on day 2 without CALI and tested on day 3, ruling out any nonspecific interference with neuronal function. Animals expressing either CFL-GFP or unfused SN formed memories as normal even in the presence of illumination. Likewise, animals expressing CFL-SN

in the absence of illumination also formed a robust memory, ruling out the possibility that overexpression of CFL-SN contributes to the observed effects.

CALI was triggered at various time points after the shock. Memory was significantly impaired when CALI was conducted within 20 min after the shock (Fig. 2D). However, memory was not impaired when the light was delivered either 1 min before the animals were placed in the IA chamber or 1 hour after the shock.

To test the context specificity of the impaired memory, we prepared two IA contexts that differed in size, floor texture, visual cues, illumination color, and odor (Fig. 2E). Mice were first trained in context A without CALI. Two hours later, mice were placed in context B where they displayed a short crossover latency, indicating that they could sufficiently distinguish context B from context A (Fig. 2E). After crossover, the mice were shocked and CALI was subsequently conducted. The next day, when returned to context B, mice that underwent CALI displayed shorter crossover latencies, indicating that the memory for context B was erased. However, when placed in context A, the same mice had crossover latencies similar to those of the control mice that did not receive CALI, demonstrating that context-specific memories can be selectively impaired.

Optical erasure of LTP during sleep also impairs memory

Hippocampal neuronal activity patterns associated with memory formation are subsequently replayed offline while animals are stationary or asleep, a process thought to underlie memory consolidation (*15*–*20*). However, it remains unknown whether such activity induces additional LTP in the brain; if it does, it is also unknown when and where this occurs. To establish whether additional LTP is induced offline (offline LTP) locally in the hippocampus during extended periods after learning, we illuminated the hippocampus every 20 min (the temporal resolution of the CFL-SN system) after the mice were returned to the home cage, starting 2 hours after the shock and continuing for 8 hours. We found that the memory was totally erased (Fig. 3A). When the same group of mice were shocked on day 2 and tested on day 3, the animals exhibited normal memory, ruling out nonspecific tissue damage. To further narrow down the time window of LTP, light was delivered either in the first or second 4-hour period. The memory was still erased, though to a lesser extent in both time windows. Because local hippocampal LTP was still contributing to memory formation in the home cage up to 8 hours after the shock, we next tested whether offline LTP extends over days. We illuminated the hippocampus only on day 2, but observed no degradation of memory (Fig. 3B), suggesting that offline LTP extends more than 2 hours after learning, but consolidation is restricted to a single day locally within the hippocampus.

Hippocampal replay occurs during both wakefulness and sleep, and it has been suggested that events in these states may serve differential roles (*19*). We analyzed the state-dependent contribution of these processes relative to the memory consolidation process. electroencephalography (EEG) and electromyography (EMG) data were analyzed online

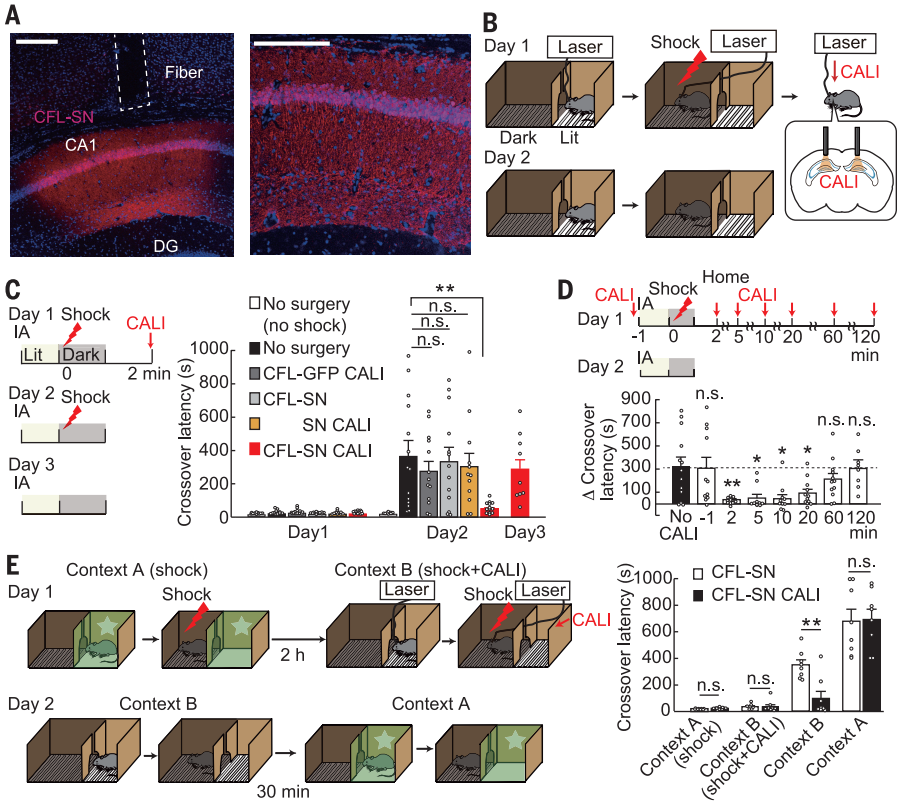

Fig. 2. Optical erasure of memory by CALI. (**A**) Distribution of CFL-SN expressed by AAV vector in dorsal CA1 pyramidal neurons (immunostained); the optical fiber tract is indicated by a dashed line in the cortex. An AAV viral vector carrying EF1α-DIO-CFL-SN was injected bilaterally into the dorsal CA1 of CaMKIIα-Cre transgenic mice. DG, Dentate gyrus. Scale bars, 300 μm. (**B**) Experimental protocol for inhibitory avoidance testing. (**C**) Erasure of memory by CALI of CFL-SN. Bar graph shows the average crossover latency in inhibitory avoidance test. Mice without virus injection or shock (no shock, n = 10), mice without virus injection but shocked (No surgery, n = 14), mice expressing CFL-GFP, shocked and illuminated (CFL-GFP CALI, n = 13), mice expressing CFL-SN, shocked but not illuminated (CFL-SN, n = 12), mice expressing SN, shocked and illuminated (SN CALI, n = 12), mice expressing CFL-SN and illuminated (CFL-SN CALI, n = 13). A subset of the last group was shocked again on day 2 but without illumination and tested on day 3 (CFL-SN CALI, n = 9). All groups except the no shock group on day 2 were statistically analyzed using one-way ANOVA tests followed by Tukey-Kramer post hoc tests (versus no surgery). P = 0.885 (CFL-GFP CALI), P = 0.998 (CFL-SN), P = 0.986 (SN CALI), P = 0.0156 (CFL-SN CALI), $F_{4,60}$ = 3.26. (**D**) Time-window of the effect of CALI of CFL-SN. CALI of CFL-SN was carried out at various time points before and after shock. Mice without CALI (n = 10), CALI 1 min before shock (n = 10), CALI 2 min (n = 10), 5 min (n = 10), 10 min (n = 10), 20 min (n = 10), 60 min (n = 10), and 120 min (n = 10) after shock. One-way ANOVA test followed by Tukey-Kramer post hoc test (versus noCALI group). P = 1, P = 0.0042, P = 0.0171, P = 0.0103, P = 0.0478, P = 0.797, P = 1 (the order is the same as in the figure), $F_{7,82}$ = 5.36. (**E**) Context selectivity of the effect of CALI. The IA test was carried out in two distinct contexts: A and B. CALI was induced 2 min after shock in context B but not in context A. Summary of crossover latency in each context with CALI (n = 8) and without CALI (n = 8). Wilcoxon signed-rank test, P = 0.1105 (Context A+shock), P = 0.314 (Context B+shock+CALI), P = 0.004 (Context B), P = 0.9591 (Context A). Means ± SEMs are shown; significance is indicated in the figures as follows: *: P < 0.05; **: P < 0.01; n.s., not significant.

to automatically determine the behavioral state of the animal (*21*), and CALI was triggered separately during either awake or sleep periods that extended for at least 20 min (Fig. 3C and fig. S6). When CALI was conducted during sleep, memory was impaired (Fig. 3D). However, when it was restricted to awake periods, no impact was evident. Further, when CALI was specifically performed during sleep periods but only on day 2, it no longer impaired memory formation (Fig. 3D). Our intervention used a similar total number of illuminations across conditions (Fig. 3E) and did not alter the patterns or periods of the sleep and wake states (fig. S7).

Differential roles of online and offline LTP on the formation of hippocampal representation

So far we have demonstrated that two forms of hippocampal LTP are required for memory formation: online LTP that takes place during or immediately after the event and offline LTP that takes place during the subsequent sleep period. We next sought to establish whether these two forms of LTP have differential impacts on hippocampal representations. We imaged Ca^{2+}-responses in hippocampal excitatory neurons of active mice using a head-mounted miniaturized fluorescence microscope (*22*). AAV_9-CAG-DIO-CFL-SN-P2A-GCaMP6f was injected into the dorsal hippocampus of CaMKIIα-Cre mice, after which a gradient index (GRIN) lens was implanted directly above the injection site (Fig. 4A). On day 1, neuronal activity was recorded when the mice were exposed to the IA chamber without shock (Fig. 4B). On day 2, mice were reexposed to the same chamber and shocked after entering the dark side. In one group of mice, light was illuminated through the lens 2 min after the shock to erase online LTP (online CALI group). To limit the effect on the local circuit, we induced CALI unilaterally on the observed side (fig. S8). In a second group, light was illuminated every 20 min—starting 2 hours after the IA test for a total of 8 hours—to erase offline LTP (offline CALI group), whereas control groups were shocked but did not receive illumination (shock noCALI group). On day 3, all three groups were reexposed to the IA test chamber and neuronal activity was recorded. We compared the firing of individual neurons in the habituation chamber and in the IA test chamber by defining a selectivity score for each cell (see methods; Fig. 4, C to E; and fig. S9A).

CA1 neurons in animals that did not receive the shock showed modest selectivity for the test chamber compared with the habituation chamber at similar levels on both day 1 and 2 (fig. S9 and Fig. 4D). By contrast, in animals that received shock (shock noCALI group), neurons fired significantly more in the test chamber than in the habituation chamber on day 3 compared with day 1, resulting in an increase in overall selectivity (fig. S9 and Fig. 4, C to E). When online LTP was erased 2 min after the shock (shock+online CALI group), increased selectivity failed to emerge. By contrast, erasure of offline LTP did not impair the increased selectivity (shock+offline CALI group).

To dissect the impact of offline LTP on the hippocampal synaptic circuit, we analyzed the population Ca^{2+} dynamics using principal component analysis (PCA) (*23*) (Fig. 4F). In the shock-only mice, after IA learning we observed that activity repeatedly deviated from the trajectories of day 1. In epochs where these deviations were observed, Ca^{2+} signals increased in multiple cells shared between the epochs (Fig. 4G), indicating that they reflect the recurring synchronous activity of specific sets of neurons. We confirmed that synchronous events occurred primarily when the deviations were observed and that the number of synchronous events increased after the shock, though the mean firing rate did not change between days 1 and 3 (Fig. 4H). The deviation in PCA, as well as the increase in synchronous events, were not evident when either online LTP or offline LTP were erased (Fig. 4, F and H, and fig. S10C), indicating the importance of both forms of LTP for synchronous activity after learning. Before door opening on day 3, synchronous firing was observed broadly around the center of the chamber, whereas after door opening, it was most pronounced adjacent to the door (Fig. 4I and fig. S10, A and B). This suggests that such assembly activity may reflect recall of the training episode. CALI eliminated such

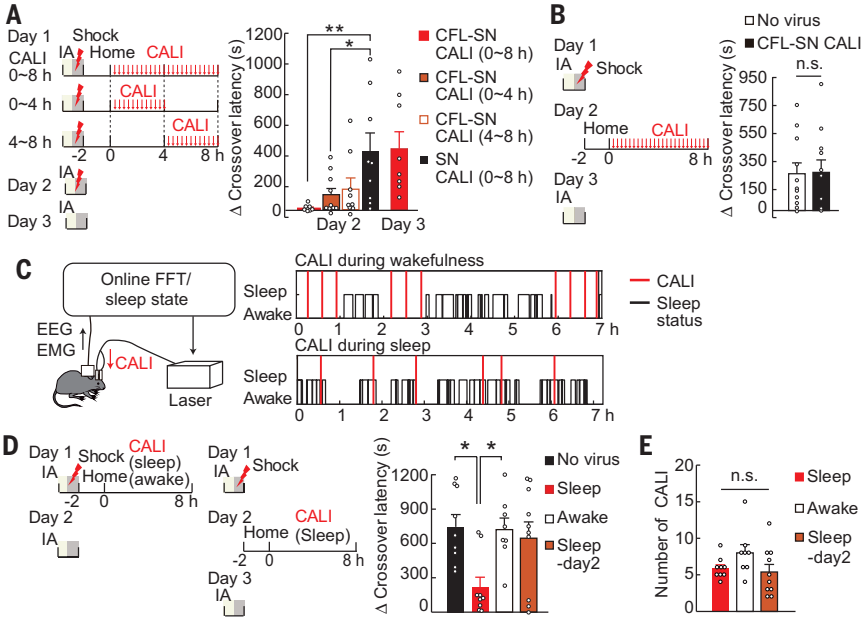

Fig. 3. Offline LTP in the hippocampus during sleep is required for memory. (**A**) Repeated CALI in the home cage erased memory. Light was delivered while animals were in the home cage every 20 min for 8 hours, either 2 hours after shock (n = 8), the first 4 hours (n = 10), or the second 4 hours (n = 9). Animals only expressing SN were illuminated and used as a control (n = 9). Animals received 8 hour repeated illumination, and shock was given again on day 2 without CALI; memory was then retested on day 3 (n = 8). One-way ANOVA test followed by the Tukey-Kramer post hoc test (versus SN CALI). P = 0.0079 (0 to 8 h), P = 0.0425 (0 to 4 h), P = 0.1153 (4 to 8 h), $F_{3,32}$ = 4.53. (**B**) Same as in (A) except that CALI was conducted the next day and memory was tested on day 3 (CFLSN-CALI, n = 11). Control mice did not express CFL-SN (No virus, n = 10). Wilcoxon signed-rank test, P = 0.843. (**C**) Automatic detection of behavioral state. EEG and EMG were recorded and analyzed online using a fast Fourier transform (FFT) every 4 sec. Light was illuminated during sleep or wake periods lasting for ≥20 min. Examples of sleep states and light illumination (red line) are shown on the right. (**D**) CALI of CFL-SN erases memory during sleep on the same day, but not the next day. Light was illuminated either during sleep (Sleep, n = 9) or wake (Awake, n = 8) periods commencing 2 hours after shock, and mice were returned to the IA box again on day 2. Control mice did not undergo CALI (No virus, n = 9). The experimental group (Sleep-day 2, n = 10) received light during sleep on the next day and were returned to the IA box on day 3. One-way ANOVA test followed by Tukey-Kramer post hoc test (versus Sleep), P = 0.0135 (No virus), P = 0.0251 (Awake), $F_{3,32}$ = 4.59. (**E**) Average number of CALI was not different among Sleep, Awake, and Sleep-day 2 groups. One-way ANOVA test, P = 0.1449. Means ± SEMs are shown; significance is indicated in the figures as follows: *: P < 0.05; **: P < 0.01; n.s., not significant.

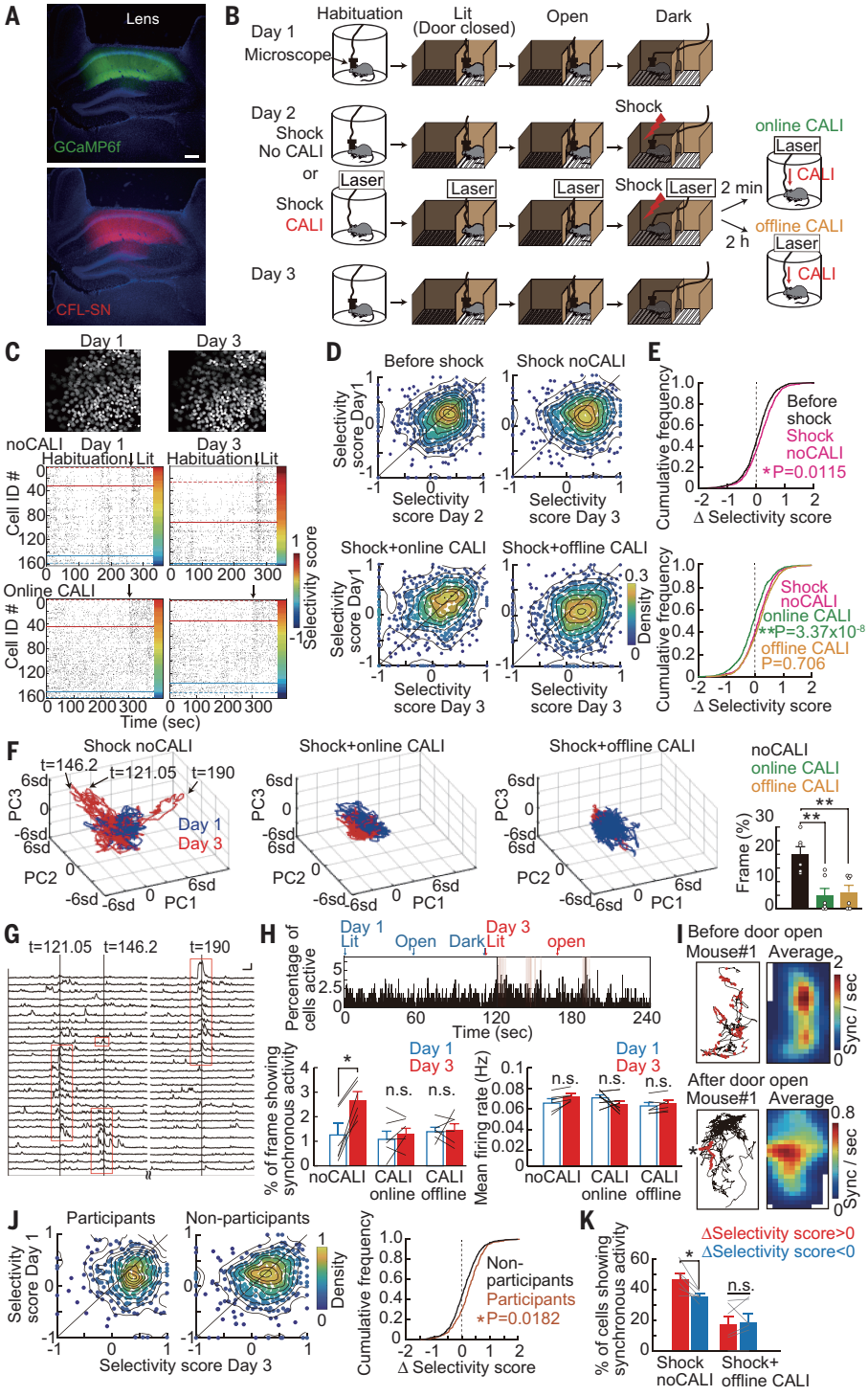

Fig. 4. Hippocampal online LTP and offline LTP have distinct roles in memory engram formation. (**A**) Expression of CFL-SN and GCaMP6f by AAV_9-CAG-DIO-CFL-SN-P2A-GCaMP6f in CA1 pyramidal neurons. (**B**) Experimental protocol of Ca^{2+} imaging during IA testing and CALI. (**C**) Images of detected cells on day 1 (before shock) and on day 3 (after shock) from a Shock noCALI mouse. Raster plot of representative cells commonly active on day 1 and day 3. Ca^{2+} events (>2 events) are plotted per sec and cells are sorted in order of selectivity score on each day. Red and blue horizontal lines indicate selectivity scores of 0.4 and -0.4, and dotted lines indicate scores of 0.8 and -0.8. Shock noCALI (top) and Shock+online CALI (bottom) mice. Raw values are shown in fig. S9B. (**D**). Selectivity score of cells on day 1 versus day 2 (Before shock, 852 cells, n = 6 mice) or on day 1 versus day 3 (Shock noCALI, 776 cells, n = 6 mice, Shock+CALI online, 763 cells, n = 6 mice, Shock+CALI offline, 935 cell, n = 6 mice) are shown. Density of plot is displayed in pseudocolor, with contours depicted as black lines. (**E**) Same data as in (D) but differences in selectivity scores are plotted in cumulative histograms. Kolmogorov-Smirnov test: No shock versus Shock noCALI (top), and with respect to control (Shock noCALI) (bottom). (**F**) Principal component analysis (PCA) of concatenated Ca^{2+} traces of day 1 and day 3 data from a mouse shocked on day 2 without CALI (left). Population trajectories were projected onto the first three principal components. Arrows indicate time points with high deviation on day 3. 6sd denotes 6 times standard deviation (SD) of PCA score on day 1. Similar PCA analysis from a mouse shocked on day 2 that underwent CALI 2 min after shock to cancel online LTP (Shock+online CALI, middle), and a mouse shocked on day 2 that underwent CALI in the home cage to cancel offline LTP (Shock+offline CALI, right). The bar graph displays the average percentage of frames that showed PCA scores on day 3 that had >3 SD of the PCA score on day 1. One-way ANOVA test followed by Tukey-Kramer post hoc test (versus Shock noCALI, n = 6 mice). P = 0.0028 (Shock+online CALI, n = 6 mice), P = 0.0058 (Shock+offline CALI, n = 6 mice), $F_{2,15}$ = 10.04. (**G**) Sample traces of neurons from a Shock noCALI mouse in (F). (t = 121.05, 146.2, and 190). Red rectangles indicate activation at those time points. Scale: 50% ΔF/F, 5 s. (**H**) Percentage of cells active on day 1 and day 3 (top). The red area indicates frames where high deviation was observed in (F). Percent of frame showing synchronous activity (bottom left) and mean firing rate (bottom right) on day 1 and day 3. Paired t-test, *P < 0.05. (noCALI, n = 6 mice, CALI 2 min, n = 6 mice, CALI Sleep, n = 6 mice). (**I**) Synchronous firing is selectively seen near the door to the dark side. Trajectory (black line) and location where high deviation was observed in PCA analysis (red dots) from a representative shock-only mouse on day 3, before and after the door opened (left). Heat map of average synchronous activity rate in lit chamber on day 3 (right). The number of synchronous activities detected by PCA analysis in each bin was pooled from 6 mice and divided by total their occupancy time in each bin. The asterisk indicates door location. (**J**) Selectivity score from cells that participated in synchronous activity were increased after shock, but no increase was observed for those that did not participate in synchronous activity. Cells that were activated (>4 SD of basal Ca^{2+} signal) at least once in the frame when high deviation was observed by PCA analysis were classified as participants. (Participant, n = 309, nonparticipant n = 467 from 6 mice). Kolmogorov-Smirnov test. (**K**) Percent of cells showing synchronous activity in the group of cells showing a higher selectivity score after shock (red bar, cells below the diagonal line in Fig. 4D) and that in the group of cells showing lower selectivity score after shock (blue bar, cells beyond the diagonal line). Paired t-test, P = 0.014, n = 6 mice (noCALI), P = 0.669, n = 6 mice (offline CALI). Means ± SEMs are shown; significance is indicated in the figures as follows: *: P < 0.05; **: P < 0.01; n.s., not significant.

accumulation (fig. S10, A and B). We then classified neurons in the noCALI group into two classes based on their participation in synchronous events using PCA analysis, then separately calculated selectivity scores (Fig. 4J). Cells that participated in synchronous activity at least once displayed a higher selectivity score after learning (day 3) than before (day 1), although those that did not exhibited a significant reduction in the degree to which the selectivity score was modulated by learning. We then classified the cells into two groups based on the changes in selectivity score before and after shock (Fig. 4K). In noCALI animals, cells that showed an increase in selectivity score after shock were more likely to participate in synchronous activity than those that showed a decrease. In offline CALI animals, the fraction of cells participating in synchronous activity was overall lower than that of noCALI animals and was comparable between cells showing an increase in selectivity score after shock and those showing a decrease. These results are indicative of a causal relationship between selectivity score and synchronous activity, which can be erased by offline CALI.

Erasure of LTP in ACC during sleep on the following day impairs memory

Finally, we attempted to better understand the process of memory transfer to the cortex by focusing on the anterior cingulate cortex (ACC), which is activated during recall of remote memory (*24*–*26*). CFL-SN was expressed in ACC excitatory neurons using AAV_2-EF1α-DIO-CFL-SN in CaMKIIα-Cre mice, and optical fibers were bilaterally implanted above ACC (Fig. 5). First, we explored the time window of synaptic plasticity within the ACC. In contrast to CALI in the hippocampus, CALI in the ACC that was triggered either 2 min after shock (Fig. 5) or every 20 min for 8 hours (commencing 2 hours after shock) did not impair memory expression (Fig. 5). By contrast, when CALI was induced every 20 min for 8 hours on day 2 and memory was assessed on day 3, we observed a robust erasure of the memory (Fig. 5). However, this was not the case when the manipulation was performed on day 25 (Fig. 5). When illumination in the ACC was restricted to either sleep or awake periods on day 2, memory could be effectively erased only during sleep (Fig. 5), demonstrating that plasticity in the ACC occurs 1 day after learning and most likely reflects the mechanism by which memories are transferred from the hippocampus to the ACC.

We developed a versatile optogenetic method allowing for the selective optical erasure of LTP in a spatially and temporally restricted manner. It effectively erases established LTP, without altering basal transmission or interfering with future LTP. This is different from other genetic or pharmacological approaches, where temporal or cell-type specificities are difficult to attain (*27*, *28*). Although other tools exist that can erase LTP, such as AS-PARac, PA-AIP, and eosin-tagged AMPA receptor antibody (*29*–*31*), our method is able to erase the early phase of LTP. This differs from AS-PARac, which is aimed at the late protein synthesis phase of LTP, as it has a much wider temporal window of intervention than PA-AIP (~1 min). It is also purely genetically encoded, unlike the eosin-tagged antibody, making it an effective method for in vivo manipulation of memories.

We found that hippocampal LTP occurs as two distinct temporal processes: online immediately after learning and offline during periods of sleep. These two processes have distinct roles: Online LTP establishes the selectivity of neuronal firing to the shock context, as previously reported (*32*), and offline LTP is predominantly responsible for the recruitment of those neurons into repeated bouts of synchronized firing. Synchronized activity was observed when animals looked into the dark side of the chamber but did not enter, possibly reflecting recall of the shock context. Our results indicate that this synchronous activity induces further LTP in neurons, which serves to stabilize the nascent memory engram encoding the abstract features encompassing an episode.

After the two waves of LTP in the hippocampus, a third wave of extra-hippocampal LTP takes place during sleep the next day in the ACC; this is required for systems consolidation. On the other hand, LTP in the hippocampus is no longer required for memory recall. Our data are consistent with a recent study that demonstrated the rapid generation of immature engram cells after training in the prefrontal cortex (*33*). They proposed that a memory engram can be formed as early as after 1 day in the ACC, but remains silent. Subsequent consolidation is required to become a fully mature engram (*2*, *33*). The density of dendritic spines consistently remains unchanged in ACC after one day but subsequently increases, possibly reflecting the maturation process, and is required for memory consolidation (*34*). In our study, the reversal of ACC plasticity on day 2 had already impaired memory 24 hours later, suggesting that even at this early point in systems consolidation, cortical circuits can play a role in memory recall. The discrepancy between our study and that of Kitamura *et al.* (*33*) is not clear at this point, but it may be due to differences in the method of inactivation (tetanus toxin to block output versus CFL-SN to erase LTP while leaving basal activity intact).

Synaptic plasticity in ACC during sleep is also most likely mediated by replay, with the high-frequency oscillatory activity that occurs across hippocampal–cortical networks thought to be key in promoting the strengthening of synaptic connections (*35*). Reinforcing the coordination between hippocampal sharp wave

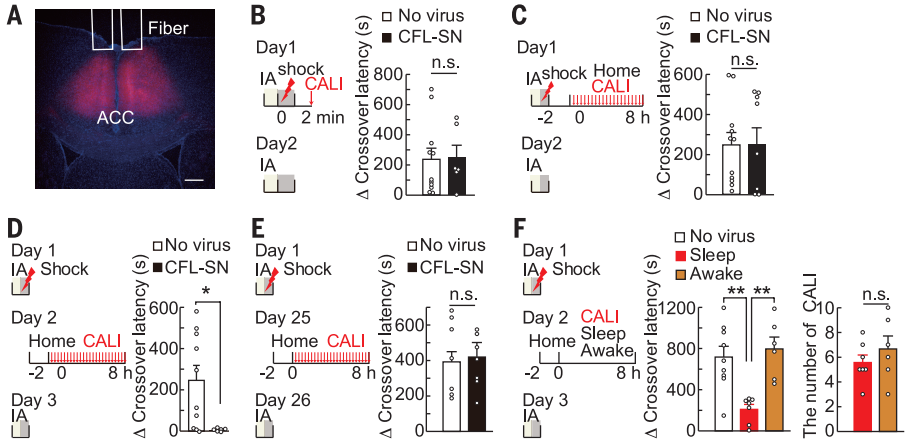

Fig. 5. ACC has an LTP time window distinct from that of the hippocampus. (**A**) Expression of CFL-SN in ACC neurons. Scale bar, 200 μm. (**B** to **E**) Effect of CALI in ACC 2 after shock. (B) 2 min, (C) 2 to 8 hours, (D) 1 day, and (E) 25 days after. Memory was erased only when CALI was performed 1 day later (2 min after; No virus, n = 11; CFLSN-CALI, n = 6. 2 to 8 hours; No virus, n = 11; CFLSN-CALI, n = 8, 1 day after; No virus, n = 10; CFLSN-CALI, n = 6. 25 days after; No virus, n = 7; CFLSN-CALI, n = 7). All experiments were done during the light cycle. Wilcoxon signed-rank tests, P = 0.81 (B), P = 0.90 (C), P = 0.025 (D), P = 0.70 (E). (**F**) Offline LTP during sleep on next day in ACC is required for memory formation. 26 hours after shock, light was illuminated either during sleep or during wake for 8 hours. All experiments were done during the dark cycle. One-way ANOVA test followed by Tukey-Kramer post hoc test with respect to sleep (n = 10), P = 0.0029 (No virus, n = 9), P = 0.0019 (awake, n = 8), $F_{2,19}$= 10.37. Average number of CALI trials did not differ between sleep CALI and awake CALI groups. Wilcoxon signed-rank test, P = 0.43. Means ± SEMs are shown; significance is indicated in the figures as follows: *: P < 0.05; **: P < 0.01; n.s., not significant.

ripples and cortical waves by electrical stimulation resulted in enhanced recall performance, whereas disruption of coupling resulted in memory impairment (*36*, *37*). Likewise, disruption of replay during sleep (*17*) has been shown to impair performance in memory-dependent tasks; however, the exact nature of the mechanisms responsible for inducing plasticity in ACC remains to be elucidated.

In conclusion, we show clear evidence that the early phase of systems consolidation is composed of multiple steps of synaptic plasticity; presumably each undergoes synaptic consolidation. Further application of the introduced optogenetic tool, possibly with color variants of SN (*38*), will allow for a more comprehensive temporal dissection of synaptic plasticity events across multiple neuronal structures and populations, thus providing a much clearer picture of memory consolidation. Although this tool was not directly shown as working for sLTP in vivo associated with learning, it may enable identification of spines that undergo synaptic plasticity during memory consolidation through combination with in vivo imaging.

REFERENCES AND NOTES

1. M. Sakaguchi, Y. Hayashi, *Mol. Brain* **5**, 32 (2012).
2. S. Tonegawa, M. D. Morrissey, T. Kitamura, *Nat. Rev. Neurosci.* **19**, 485–498 (2018).
3. J. Z. Tsien, P. T. Huerta, S. Tonegawa, *Cell* **87**, 1327–1338 (1996).
4. P. W. Frankland, C. O'Brien, M. Ohno, A. Kirkwood, A. J. Silva, *Nature* **411**, 309–313 (2001).
5. K. Okamoto, T. Nagai, A. Miyawaki, Y. Hayashi, *Nat. Neurosci.* **7**, 1104–1112 (2004).
6. M. Bosch *et al*., *Neuron* **82**, 444–459 (2014).
7. E. Andrianantoandro, T. D. Pollard, *Mol. Cell* **24**, 13–23 (2006).
8. J. R. Bamburg, A. McGough, S. Ono, *Trends Cell Biol.* **9**, 364–370 (1999).
9. K. Takemoto *et al*., *Sci. Rep.* **3**, 2629 (2013).
10. K. Kim *et al*., *Neuron* **87**, 813–826 (2015).
11. E. A. Vitriol, A. L. Wise, M. E. Berginski, J. R. Bamburg, J. Q. Zheng, *Mol. Biol. Cell* **24**, 2238–2247 (2013).
12. N. Honkura, M. Matsuzaki, J. Noguchi, G. C. Ellis-Davies, H. Kasai, *Neuron* **57**, 719–729 (2008).
13. Q. Zhou, K. J. Homma, M. M. Poo, *Neuron* **44**, 749–757 (2004).
14. Z. Zhou, J. Hu, M. Passafaro, W. Xie, Z. Jia, *J. Neurosci.* **31**, 819–833 (2011).
15. M. A. Wilson, B. L. McNaughton, *Science* **265**, 676–679 (1994).
16. D. Nakayama *et al*., *J. Neurosci.* **35**, 819–830 (2015).
17. G. Girardeau, K. Benchenane, S. I. Wiener, G. Buzsáki, M. B. Zugaro, *Nat. Neurosci.* **12**, 1222–1223 (2009).
18. L. A. Atherton, D. Dupret, J. R. Mellor, *Trends Neurosci.* **38**, 560–570 (2015).
19. Z. Chen, M. A. Wilson, *Trends Neurosci.* **40**, 260–275 (2017).
20. K. Ghandour *et al*., *Nat. Commun.* **10**, 2637 (2019).
21. D. Miyamoto *et al*., *Science* **352**, 1315–1318 (2016).
22. Y. Ziv *et al*., *Nat. Neurosci.* **16**, 264–266 (2013).
23. P. Rajasethupathy *et al*., *Nature* **526**, 653–659 (2015).
24. B. Bontempi, C. Laurent-Demir, C. Destrade, R. Jaffard, *Nature* **400**, 671–675 (1999).
25. P. W. Frankland, B. Bontempi, L. E. Talton, L. Kaczmarek, A. J. Silva, *Science* **304**, 881–883 (2004).
26. Y. Zhang, H. Fukushima, S. Kida, *Mol. Brain* **4**, 4 (2011).
27. G. Riedel *et al*., *Nat. Neurosci.* **2**, 898–905 (1999).
28. E. Shimizu, Y. P. Tang, C. Rampon, J. Z. Tsien, *Science* **290**, 1170–1174 (2000).
29. A. Hayashi-Takagi *et al*., *Nature* **525**, 333–338 (2015).
30. H. Murakoshi, H. Wang, R. Yasuda, *Nature* **472**, 100–104 (2011).
31. K. Takemoto *et al*., *Nat. Biotechnol.* **35**, 38–47 (2017).
32. K. Z. Tanaka *et al*., *Science* **361**, 392–397 (2018).
33. T. Kitamura *et al*., *Science* **356**, 73–78 (2017).
34. G. Vetere *et al*., *Proc. Natl. Acad. Sci. U.S.A.* **108**, 8456–8460 (2011).
35. K. Takehara-Nishiuchi, *Brain Neurosci. Adv.* **4**, 2398212820925580 (2020).
36. N. Maingret, G. Girardeau, R. Todorova, M. Goutierre, M. Zugaro, *Nat. Neurosci.* **19**, 959–964 (2016).
37. F. Xia *et al*., *eLife* **6**, e27868 (2017).
38. Y. D. Riani, T. Matsuda, K. Takemoto, T. Nagai, *BMC Biol.* **16**, 50 (2018).

ACKNOWLEDGMENTS

We thank K. Okamoto and M. Bosch for their contribution in the conceptualization of this work; P. Frankland, S. Kida, S. Middleton and T. Toyoizumi for comments; T. Manabe for help in setting up field recording; Y. Nishiyama for help in PCA analysis; and I. Nakahara (Neuro Programming Research) for writing the custom MATLAB program used in the sleep experiment. **Funding:** Grant-in-Aid for Scientific Research JP21650080, JP16H01292, JP16H01438, JP16H02455, JP17K19631, JP18H05434, and JP19H01010 from the MEXT, Japan, was given to Y.H. Grant-in-Aid for Scientific Research JP19H05233 was given to T.J.M. Grant-in-Aid for Scientific Research JP15K06728, JP17H05949, JP18K14818, and JP20K15901 from MEXT, Japan, was given to A.G. Grant-in-Aid for JSPS Research Fellow supported A.G. Grant-in-Aid for Scientific Research JP18H05410 from MEXT, Japan, was given to T.N. The Uehara Memorial Foundation supported Y.H., and the Naito Foundation supported Y.H. and T.N. Research Foundation for Opto-Science and Technology, Novartis Foundation, and the Takeda Science Foundation supported Y.H.; Y.H. also received HFSP Research Grant RGP0022/2013. JST CREST JPMJCR20E4 was given to Y.H. and T.M. JST Presto JPMJPR0165 was given to T.N. Inamori Grants from the Inamori Foundation were given to T.N. **Author contributions:** Conceptualization: A.G. and Y.H. Methodology: A.G., D.H., M.M., T.M., T.N., and Y.H. Investigation: A.G., A.B., K.M., J.W., S.T., X.J., and Y.H. Visualization: A.G. and Y.H. Funding acquisition: A.G., T.M., T.N., and Y.H. Project administration: Y.H. Supervision: Y.H. and T.J.M. Writing – original draft: A.G. and Y.H. Writing – review and editing: T.J.M. **Competing interests:** Y.H. is partly supported by Fujitsu Laboratories and Dwango. **Data and materials availability:** All data are available in the main text or in the supplementary materials. The gene for SuperNova is available from Addgene as SuperNova/pRSETB (#53234).

SUPPLEMENTARY MATERIALS

science.org/doi/10.1126/science.abj9195
Materials and Methods
Figs. S1 to S10
References (*39*, *40*)
MDAR Reproducibility Checklist

View/request a protocol for this paper from Bio-protocol.

10 June 2021; accepted 24 September 2021
10.1126/science.abj9195

Stepwise synaptic plasticity events drive the early phase of memory consolidation

Akihiro GotoAyaka BotaKen MiyaJingbo WangSuzune TsukamotoXinzhi JiangDaichi HiraiMasanori MurayamaTomoki MatsudaThomas J. McHughTakeharu NagaiYasunori Hayashi

Science, 374 (6569), • DOI: 10.1126/science.abj9195

Where and when of memory consolidation

Episodic memory is initially encoded in the hippocampus and later transferred to other brain regions for long-term storage. Synaptic plasticity underlies learning and plays a critical role in memory consolidation. However, it remains largely unknown where and when synaptic plasticity occurs and how it shapes the neuronal representation. Goto *et al*. developed a new tool for controlling early structural long-term potentiation (sLTP). By selectively manipulating sLTP, the authors showed that the local circuitry in hippocampal area CA1 is required for memory formation shortly after the encoding event. The local circuitry is also important for offline memory consolidation within 24 hours. The anterior cingulate cortex, another brain region directly connected with area CA1, is crucial for memory consolidation during sleep on the second night. —PRS

Science
AAAS

Supplementary Materials for

Stepwise synaptic plasticity events drive the early phase of memory consolidation

Akihiro Goto *et al.*

Corresponding author: Yasunori Hayashi, yhayashi-tky@umin.ac.jp

Science **374**, 857 (2021)
DOI: 10.1126/science.abj9195

The PDF file includes:

Other Supplementary Material for this manuscript includes the following:

Materials and Methods

Animals.

Animal experiments were conducted in accordance with the guidelines of the Committees for Animal Care of Kyoto University and RIKEN. Mice were housed in groups of one to five per cage with littermates, with a 12 h light/dark cycle and *ad libitum* access to food and water. Mice were single housed post-surgery and throughout the rest of the experiments. All animals were between 10-25 weeks-old, and either wild-type male C57BL/6JJmsSlc mice (WT: SLC) or CaMKIIα-Cre transgenic male mice (Jackson Laboratory; strain Tg (Camk2a-cre) T29-1Stl) (*3*).

Hippocampal slice culture and gene transfection.

Hippocampal organotypic slice cultures were prepared from postnatal day 6-7 rats (*5*). Slices were cultured at 35 ºC on interface membranes (Millipore) and fed with MEM media containing 20% horse serum, 27 mM D-glucose, 6 mM $NaHCO_3$, 2 mM $CaCl_2$, 2 mM $MgSO_4$, 30 mM HEPES, 0.01 % ascorbic acid and 1 μg/ml insulin. pH was adjusted to 7.3 and osmolality to 300-320 mOsm. Slices were biolistically transfected (BioRad) after 5-7 DIV with a plasmid expressing GFP, DsRed2, CFL-GFP, CFL-SN and PAGFP-β-actin under the CAG promoter.

2P microscopy imaging, induction of sLTP in single spines and CALI.

Time-lapse fluorescence imaging was carried out with a 2P microscope (FluoView FV1000MPE, Olympus) equipped with two mode-lock femtosecond-pulse Ti:sapphire lasers (MaiTai HP, Sprectra-Physics). Slices were maintained at room temperature (r.t., 25-27°C) in a continuous perfusion of artificial cerebrospinal fluid (ACSF) containing 119 mM NaCl, 2.5 mM KCl, 3 mM $CaCl_2$, 26.2 mM $NaHCO_3$, 1 mM NaH_2PO_4 and 11 mM glucose, 1 μM tetrodotoxin, 50 μM picrotoxin and 6 mM 4- methoxy-7-nitroindolinyl (MNI)-L-glutamate (Tocris, Bristol, UK) equilibrated with 5% CO_2/95% O_2. A subset of experiments was carried out with 2.5 mM MNI-glutamate and increased (4 mM) $CaCl_2$ concentration. Imaging was performed at 8-9 DIV in primary or secondary dendrites from the distal part of the main apical dendrite of CA1 pyramidal neurons. To avoid overexpression issues, we selected only neurons that had a minimal GFP or DsRed2 signal when excited at 910 nm, but were bright enough to image above noise. Additionally, we ensured that all neurons had typical dendritic morphology and displayed no sign of fluorescent aggregates. Expression of CFL-SN or SN was confirmed at the conclusion of experiments to avoid inadvertent induction of CALI prior to recording, and likewise dendritic morphology was reassessed to confirm neurons remained healthy. sLTP was induced only on thin or small mushroom spines, with a clearly visible head and neck. 2P uncaging of MNI-glutamate was performed using 720 nm light (5 mW), with green and red fluorescence proteins simultaneously excited at 910 nm. Both lasers were aligned daily by imaging and bleaching 0.5 μm fluorescent beads (Invitrogen). sLTP was induced by 1 ms pulses repeated at 1 Hz for 1 min targeted close to the tip of the spine, as previously described (*6*).

For PAGFP experiments, the timing and duration of pulses were as previously explained (*12*). Laser irradiation was focused at a point 0.3–0.5 mm from the tip of a spine and repeated 60 times at 1 Hz with a pulse duration of 0.6 ms. We then collected images of activated PAGFP-actin and DsRed with illumination at 910 nm.

For induction of CALI at 559 nm, a square region (2 μm x 2 μm, 100 pixels x 100 pixels) around the stimulated spine was repeatedly scanned with 559 nm laser (100 μW, LUMPlanFI/IR, 60X/0.90 W, Olympus, 2 μs per pixel dwell time) for 30 sec. For induction of CALI at 593 nm, a laser (YL593T3-030FC, Shanghai Laser & Optics Century Co.) was connected to ferrule with 0.22 NA and a 200-μm-thick protruding cleaved bare optic fiber. The optic fiber was located beside an objective lens for spine imaging and adjusted to focus onto a spot (2 mm in diameter; 0.8 W/cm^2). For the purposes of adjusting the location of fibers, a 473 nm laser (BL473, Shanghai Laser & Optics Century Co.) which does not induce CALI was used, after which it was switched to the 593 nm laser.

Image analysis of sLTP experiments

At every time-point, a series of 512 x 512-pixel XY-scanned images were taken every 1 μm of depth (Z). The fluorescence intensity of 7-10 of these images were summed to obtain a single Z-stack image. A constant region of interest was outlined around the spine including the spine head and half of spine neck and the total integrated fluorescence intensity of the green and red channels was calculated using ImageJ (National Institutes of Health). Values were background-subtracted and corrected for bleed-through and overall fluorescence fluctuations.

Preparation of Adeno-Associated Viruses

pAAV-EF1α-DIO-CFL-SN, pAAV-EF1α-DIO-SN and pAAV-EF1α-DIO-CFL-GFP were constructed by replacing the ChR2-eYFP fusion gene in the pAAV-EF1α-double foxed-hChR2(H134R)-EYFP-WPRE-HGHpA (Addgene plasmid # 20298) with a gene of CFL-SN, SN and CFL-GFP respectively. pAAV-CAG-DIO-CFL-SN-P2A-GCaMP6f was constructed by replacing pAAV-CAG-DIO-ChR2(H134R)-eYFP (Addgene plasmid # 127090) with CFL-SN-P2A-GCaMP6f. GCaMP6f was subcloned from pAAV-CAG-Flex-GCaMP6f-WPRE-SV40 (Addgene plasmid # 100835). To avoid ribosomal read-through, Gly-Ser-Gly was inserted upstream of P2A. We confirmed by western blotting that more than 80% of CFL-SN and GCaMP6f were expressed separately. These plasmids were used to generate AAV vectors. AAV_2-EF1α-DIO-CFL-SN, AAV_2-EF1α-DIO-SN and AAV_9-CAG-DIO-CFL-SN-P2A-GCaMP6f were purified by Iodixanol Gradient Ultracentrifugation (*39)*. The AAV vector used only in Figure 2C (AAV_2-EF1α-DIO-CFL-SN, The AAV_2-EF1a-DIO-SN and AAV_2-EF1a-DIO-CFL-GFP) was purified with a column which binds AAV2 particles (Takara). Viral titer was 1.7 x 10^{13} genome copies (GC) per ml for AAV_2-EF1α-DIO-CFL-SN, 1.9 x 10^{13} GC per ml for AAV_2-EF1α-DIO-SN, 1.2 x 10^{13} GC per ml for AAV_2-EF1a-DIO-CFL-GFP and 5.1 x 10^{13} GC per ml for AAV_9-CAG-DIO-CFL-SN-P2A-GCaMP6f. Among different preparation for the same

virus, viral titer was adjusted by concentrating viral solution with a filter (Millipore). AAV_2-CMV-PI-eGFP-WPRE-bGH was purchased from Penn Vector Core.

Stereotactic Injection and Fiber Optic Implants

Surgical procedures on mice were performed with isoflurane anesthesia, or 500 mg kg^{-1} Avertin (administered intraperitonially and used only in experiments described in Figure 2C). Under stereotaxic guidance, virus was injected using a glass micropipette attached to a microsyringe (MS-10; ITO) through a tube filled with liquid paraffin. 150~500 nl of virus was injected at a rate of 60 nl min^{-1}. Hippocampal CA1 stereotaxic coordinates were -2.3 mm anteroposterior (AP), 1.8 mm mediolateral (ML), and 1.4 mm dorsoventral (DV) from bregma. ACC coordinates were 0.8 mm AP, 0.3 mm ML, 1.2 mm DV. Following viral injection, the needle was held in place for an additional 10 min prior to withdrawal, after which optic fibers were implanted. For CALI, in bilateral hippocampal CA1, mice were implanted with fiber-optic lightguides consisting of a 1.25-mm diameter metal ferrule with 0.5 NA and a 200-µm-thick protruding cleaved bare optic fiber cut to the desired length (Thorlabs) at 0.15 mm dorsal to the injection site. For CALI in bilateral anterior cingulate, dual fiber-optic cannulas of 200 µm thickness and 0.22 NA spaced 0.7 mm apart (Doric Lenses) were lowered 0.2mm above the site of injection. A screw was placed into the skull anterior to the site of injection. A layer of adhesive cement (SHOFU) was applied around the optical fiber. Mice were given 1 mg kg^{-1} Ketoprofen as an analgesic. All viral injection sites were verified at the conclusion of the experiments.

Histology

Mice were transcardially perfused with 4 % paraformaldehyde (PFA) in phosphate buffered saline (PBS). Brains were post-fixed with the same solution for 24 hours, and then sectioned using a vibratome into coronal sections. For immunohistochemistry, the sections were incubated in a buffer (0.1 M Tris-HCl, 0.15 M NaCl) with 0.5 % Triton-X, 5 % blocking reagent (Roche) and primary antibodies and incubated overnight at 4°C. We used rabbit anti-KillerRed antibody (Evrogen, AB961, 1:1000) as a primary antibody to stain SN. After rinsing with PBS 3 times for 15 min each, the sections were subsequently incubated with AlexaFluor 647 conjugated secondary antibodies (Cell Signaling, 1:500) and Hoechst 33258. The sections were then washed with PBS 3 times for 15 min and mounted in VECTASHIELD antifade mounting medium. Fluorescence images were taken with a confocal microscope or with a wide-field fluorescent microscope.

Electrophysiology and CALI.

To express CFL-SN in CA1, a mixture of AAV_2-flox-CFL-SN and AAV2-CMV-PI-eGFP-WPRE-bGH was injected into 8 weeks old CaMKIIα-Cre mice, with the latter being used identify the infected area. Two weeks after injection, all procedures for slice preparation and electrophysiology recording were done under red light to avoid unintended CALI induction. Transverse hippocampal slices (400-µm thickness) were prepared using a McIlwain chopper.

Slices were illuminated with a blue flashlight and inspected for green fluorescence through yellow-colored glasses. Only slices showing green fluorescent in CA1 were used for subsequent recording. Slices were allowed to recover at room temperature for 1.5 h in artificial cerebrospinal fluid (ACSF) and aerated with 95% O_2 and 5% CO_2. Extracellular fEPSPs were recorded with a glass microelectrode (less than 5 Mohm, filled with ACSF) positioned in the *stratum radiatum* of area CA1, while green fluorescence was observed by microscope. A bipolar stimulating electrode was used to elicit fEPSPs every 6 second by stimulation of the Schaffer collateral fibers. A low pass filter (606Hz) was applied to the data and EPSP slope was measured from 10 traces of EPSP during 1 min and averaged. LTP was induced electrically by applying three 1-sec trains (100 Hz) spaced 5 sec apart. After all recordings, expression of CFL-SN (red signal) was confirmed by microscope. EPSP traces in the figures are smoothed using the filter function of MATLAB (Mathworks).
For CALI induction, the samples were exposed to light provided by Hg lamp (BP520-550, 500 μW, 3 min). Optics were adjusted to focus onto a spot (2.3 mm in diameter) on the sample.

Inhibitory avoidance test and CALI.
On the day of the test, mice were briefly anesthetized by isoflurane and optic fibers were connected to deliver 593 nm laser light. After that, the mice were acclimated to the room for at least 20 min in which experiments were to be conducted. The behavioral apparatus used in the experiments was composed of a lit chamber (10 cm (W) x 17 cm (D) x 21 cm (H)) and a dark chamber (20 cm (W) x 17 cm (D) x 21 cm (H)). The lit chamber had a metal grid floor and a white wall without a roof and was illuminated with white light (25k lux). The dark chamber had a metal grid floor and black walls without a roof was illuminated with 940 nm light, which is not visible for mice. The lit chamber was linked to the dark chamber through a sliding door. These chambers were cleaned with 70% ethanol prior to the introduction of each mouse. Mice were placed in a lit chamber for 30 seconds, and the door leading to the dark chamber was then opened. Once the mice had stepped with all four paws into the dark chamber, the door was closed. 20 seconds later, an electric footshock was delivered (0.9 mA, 50 Hz, 3 s, duration of pulse is 1 msec). After the mice were kept in the dark chamber for 1 min, the mice were then returned to their home cage. For memory retention tests, the protocol outlined above was repeated with the exception of the electric shock, and the time latencies for mice to step into the dark chamber was measured. Mice that did not enter the dark chamber within 20 minutes were excluded.
For CALI 1 min, 5min and 10 min after the IA test, mice were returned to home cage immediately after IA testing and kept in the same room until CALI was conducted. Twenty min after CALI (593 nm,1 mW at the fiber tip, 60 sec), mice were briefly anesthetized to detach optic fibers. For CALI 20 min, 60 min, 1 hour and 2 hours after IA testing, optic fibers were connected via a custom rotary joint. After IA test, mice were returned to home cage surrounded by white walls to avoid agitation. Just prior to light illumination for CALI, optic fibers were connected to the 593 nm laser without anesthetic.

For inhibitory avoidance testing during Ca^{2+} imaging, the same procedure explained above was conducted, except mice were placed in a lit chamber for 1 min before door opening and shock was delivered right after mice entered the dark room. For CALI induction through GRIN lens, 593 nm laser was illuminated from an optic fiber (400 μm thickness and 0.53 NA) which was adjusted to be in the focal plane of (500 μm away from) the lens.
For multi-context IA testing, we used two apparatuses with different sizes of box, floor texture, visual cues, color of light and odor. Context-B was a chamber with the same size used for experiment above, with flat plastic floor, visual cues, white color (25k lux) and odor of ethanol in the lit side. Context-A was a chamber (30 cm (W) x 23 cm (D) x 20 cm (H)) with a fluffy floor, another set of distinct visual cues, green color (25k lux) and odor of 0.5% acetic acid in lit side. Context-A was composed of lit and dark chambers of equal size (15 cm (W) x 23 cm (D) x 20 cm (H)).

Polysomnographic recording and CALI

Implantation of electrodes for electroencephalogram (EEG) and electromyogram (EMG) recording was performed as previously described (*21*). Briefly, an EEG screw was implanted over the parietal cortex (7.3 mm AP, 19.5 mm ML) and secured with dental cement. EEG signals were recorded and referenced against a screw implanted in skull over cerebellum. For EMG recordings, a flexible wire cable was implanted into the neck muscle.
Continuous EEG and EMG signals were recorded (Neuralynx), amplified, filtered (EEG, 0.1-50 Hz; EMG, 15–300 Hz), and digitized at a sampling rate of 1 kHz. Both recording wire and optic fibers for CALI were connected to Fiber-optic & Electrical Rotary Joints (Doric), which can transmit both electric current and light, to release the tension from twisting of the wires or cables. For habituation, mice were connected to recording wires at least 4 days prior to recording on a pedestal (22 cm diameter, 30 cm height). The animal's behavior was monitored through a USB camera and recorded on a computer. Recorded data were analyzed by custom-made MATLAB software every 4 seconds. Behavioral states (awake, NREM or REM) were identified by the algorithm previously descried (*21*). Prior to connecting optic fibers from the laser with a ferrule, laser power was adjusted so that final output was 1 mW. Photostimulation was automatically delivered to mice when conditions were met by the computer-based system.

Ca^{2+} imaging.

Ca^{2+} imaging from hippocampus was performed on CaMKIIα-Cre mice two weeks following injection of AAV_9-CAG-DIO-CFL-SN-P2A-GCaMP6f, microendoscope implant, and baseplate surgeries. Imaging was performed in right hippocampus as previously reported (*22, 40*). For habituation, dummy microscopes were mounted on mice, and the mice were housed on a pedestal (22 cm diameter, 30 cm height, termed habituation chamber during Ca^{2+} imaging) in the experimental room at least 4 days prior to recording. On the day of recording, mice were briefly anesthetized to mount the microscope, then returned to the habituation chamber. Twenty min later, recording began, and following a further 2 minutes room lights were turned off. After

further recording for 2 minutes under red light, the IA test was conducted as described above. Ca^{2+} signals from GCaMP6f were imaged during the entire exposure period and were captured at 20 Hz on a miniature microscope (nVista HD, Inscopix). At the conclusion of recording, mice were placed back to home cage and twenty minutes later were anesthetized to detach the microscope. On learning session, the microscope was not mounted and CALI was conducted unilaterally through the lens.

Image processing and cell identification across sessions.

The raw image of each frame was translated into a 16-bit TIFF image and spatially down-sampled (4-pixel bins) with an image decompressor (Inscopix). All subsequent analysis for image processing and cell identification across sessions were conducted by Inscopix Data Processing Software (Inscopix). The images were pre-processed, spatially filtered (low cut-off 0.005 $pixel^{-1}$ and high cut-off 0.5 $pixel^{-1}$), motion-corrected and transformed into $\Delta F/F$ signals. Cells were identified by PCA-ICA [240 output principal components, 200 independent components (ICs), 0.1 weight of temporal information in spatiotemporal ICA, 750 iterations maximum, 1E-5 convergence threshold]. Detected ROIs with >2 components, >70 pixels cell size and <3 SNR (the signal to noise ratio) were excluded from analysis. Ca^{2+} events were detected using the 'Event Detection' function (>4 events threshold factor and >0.4 sec decay time, negative transients were discarded). Across-session neuron registration was performed using the 'Longitudinal Registration' (>0.5 correlation) function.

Selectivity score.

We used the following formula to define the "selectivity score" in each single cell which was commonly active in day 1 and day 2, or day 1 and day 3.

$$\text{Selectivity Score} = (\text{firing rate in lit room} - \text{firing rate in habituation chamber}) / (\text{firing rate in lit room} + \text{firing rate in habituation chamber}).$$

Firing rate in the lit room was defined as the total number of activity events after mice were placed in lit room until 500 frames after the door was opened, divided by time. Firing rate in home cage was defined as the total number of activity events while mice were in the home cage just prior to the IA test, divided by time.

PCA analysis.

PCA was conducted using the MATLAB function 'pca'. PCA was applied to $\Delta F/F$ traces in day 3 concatenated with those from day 1, for each cell which was commonly active on both days (typically 150 cells per mice). Traces on day 1 were captured between the frame when mice were placed in the lit chamber to the frame when mice entered the dark chamber (typically 1200 frames). For Figures 4F-H and 4J, the same length of trace on day 3 was concatenated with it, for

the purposes of PCA analysis. For Figure 4I, traces on day 3 ranged between the frame when mice were placed in the lit chamber and the frame when the mice entered the dark chamber

Synchronous activity.

To identify synchronous activity that included more active cells than would be expected by chance at each frame, we used interval reshuffling (randomly reordering of intervals between events for each cell), performed 1,000 times for each mouse. The threshold percentage of active neurons corresponding to a significance level of $P < 0.05$ was taken to be the per cent of coactive cells required in a single frame to be considered a synchronous event, and this threshold is more than 2.5% active neurons per frame across all mice and fields of view.

Statistical analyses.

Data are expressed as means ± SEM unless otherwise stated. When only two groups were compared, paired two-tailed t tests or two-sided Wilcoxon signed-rank tests were used. When more than two groups were compared, analysis of variance (ANOVA) was used with p values adjusted for *post hoc* multiple comparisons. Significance levels were set to $P=0.05$. Significance is indicated in the figures as follows: *: $P < 0.05$; **: $P < 0.01$. Statistical details including sample sizes and exact p values are described in the figure captions.

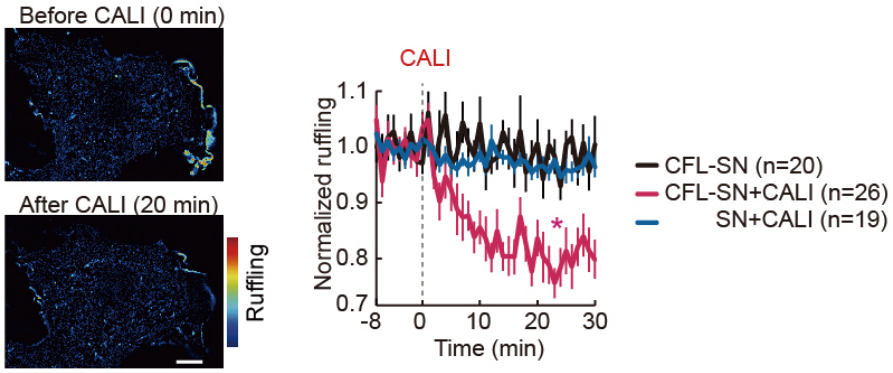

Figure S1. The effect of CALI on actin-dependent movement of lamellipodia.
Actin-dependent movement in lamellipodia of cells expressing GFP-actin is calculated as the change in GFP intensity between 2 successive time points (ruffling) and displayed as pseudocolor (left). Addition to GFP-actin, cells expressed CFL-SN or unfused SN. CALI was induced by scanning whole cells with a 559 nm (100 µW, 2 µs per pixel) laser for 3 min. A graph shows the time course of changes in ruffling, normalized to baseline. Ruffling (20-30 min) was statistically analyzed by a one-way ANOVA test followed by Tukey-Kramer post hoc test. p = 0 (SN+CALI versus CFL-SN+CALI), P=0 (CFL-SN versus CFLSN+CALI), p=0.7047 (CFL-SN versus SN+CALI), $F_{(2,62)} = 33.82$.

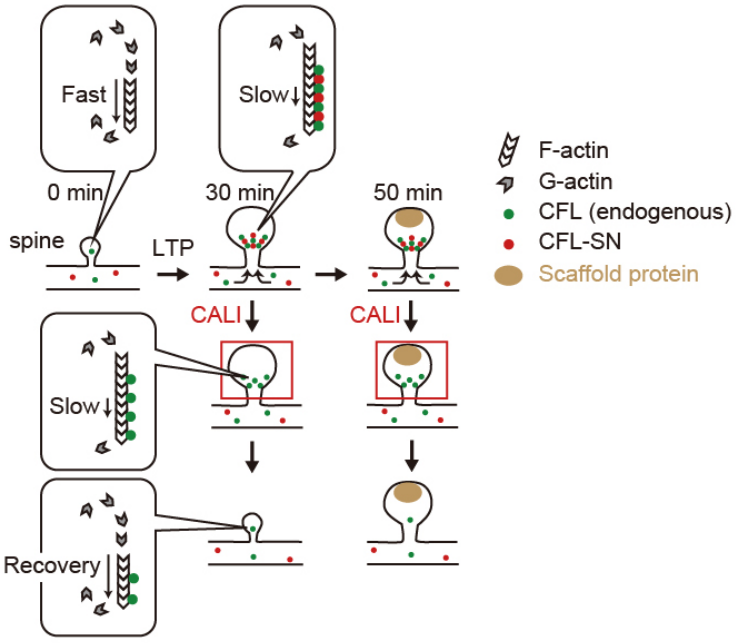

Figure S2. A molecular model for optical erasure of sLTP by CALI.
Dynamics of CFL, actin and spine structure involved in induction and erasure of sLTP. Upon induction of sLTP, CFL-SN and endogenous CFL rapidly accumulate forming a cofilactin structure in the spine, while actin turnover slows. Because of the cooperativity of the CFL molecules, CALI of CFL-SN causes a dissociation and redistribution of endogenous CFL from the dendritic spine by destabilizing the cofilactin structure, and restoring actin turnover (top). Induction of CALI 50 min after sLTP doesn't affect spine volume due to synaptic consolidation processes (bottom).

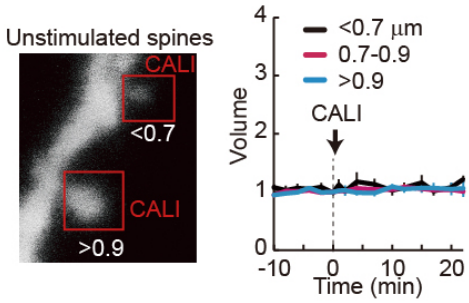

Figure S3. The effect of CALI on unstimulated spines of various sizes.
559nm laser light was illuminated on unstimulated spines of various size. Spines were classified into three groups based on size. <0.7 μm (n=12), 0.7-0.9 μm (n=12) and >0.9 μm (n=12). Spine volume (10-20 min) was statistically analyzed by a one-way ANOVA test followed by Tukey-Kramer post hoc test. $p = 0.89$.

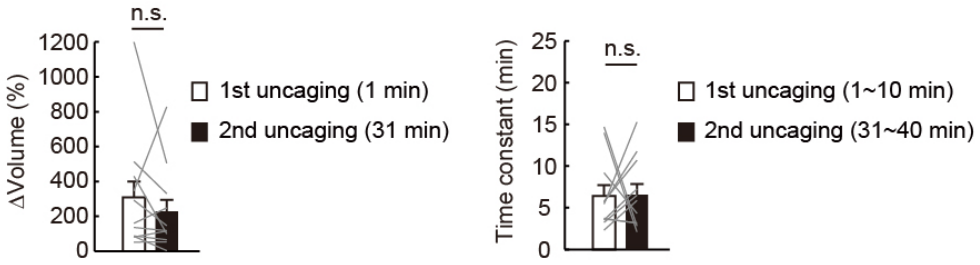

Figure S4. Comparison of volume change and decay time constant of sLTP before and after CALI.

After sLTP was induced by 1st glutamate uncaging, CALI was conducted to erase sLTP on spines expressing CFL-SN with CALI. Then LTP was induced again by the 2nd uncaging. The original data are in **Fig. 1E**.

Left: Averaged volume 1 min after 1st (before CALI) and 2nd (after CALI) uncaging. Paired t-test, p=0.38.

Right: Time constant of decay in spine volume after 1st and 2nd uncaging. Paired t-test, p=0.94.

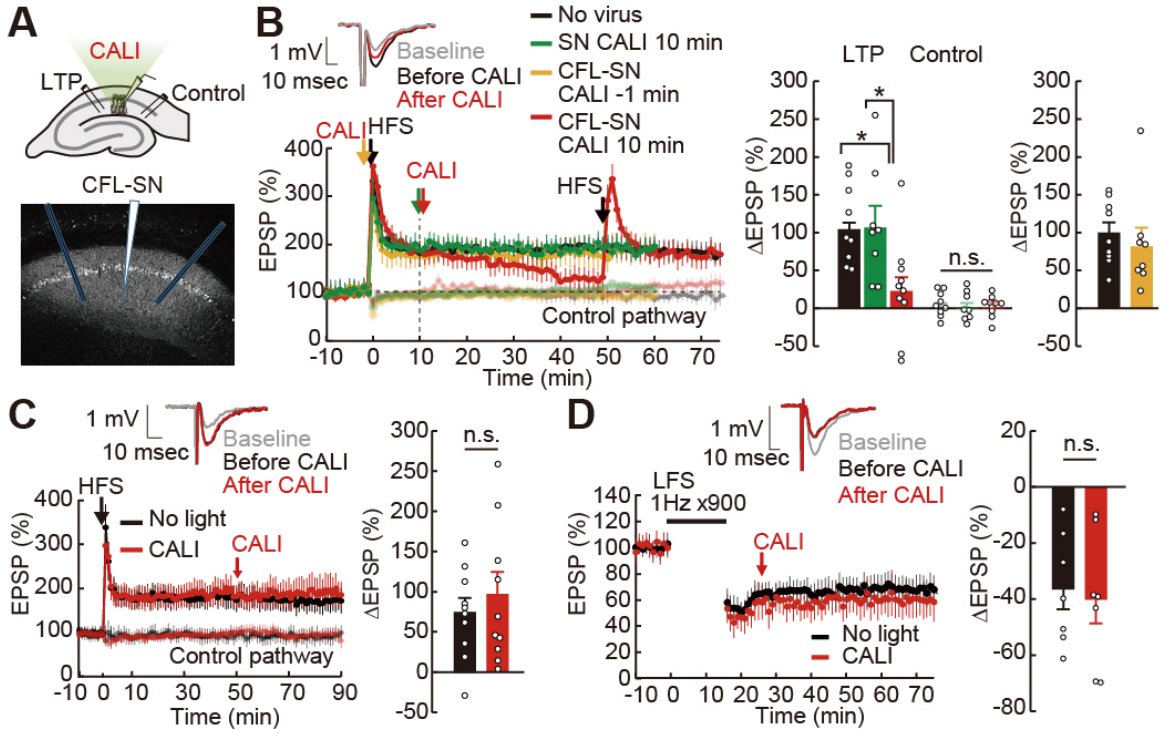

Figure S5. Optical erasure of electrically recorded LTP but not of LTD.
(**A**) fEPSPs were recorded from *stratum radiatum* of CA1 in hippocampal slices expressing CFL-SN. Light from a Hg lamp (520-550 nm band pass, 500 µW, 3 min) was used to induce CALI. A representative CFL-SN image of a slice and the positions of recording and stimulation electrodes are shown. (**B**) Effect of CALI of CFL-SN on electrically recorded LTP. Control EPSPs were recorded from mice without virus injection (n=10). CALI was induced in slices expressing CFL-SN 1 min prior to high-frequency stimulation (HFS, 100 Hz for 1sec, 3 times) (n=8), or after 10 min (n=10) or in slices expressing SN only after 10 min (n=8). Inset: examples of fEPSP traces in baseline (0 min), before CALI (10 min) and after CALI (40 min). HFS was redelivered after CALI to rule out nonspecific damage to the tissue. Bar graphs show summary in changes in fEPSP slope. Left bar graph; LTP and control pathways at 40-50 min. LTP pathway was statistically analyzed using an ANOVA test followed by Tukey-Kramer post hoc comparisons (versus CFL-SN CALI 10 min). p=0.021 (no virus), p=0.0304 (SN CALI), $F_{(2,24)}$=5.41. Control pathway was analyzed with a one-way ANOVA, p=0.88 (among 3 groups). Right bar graph; LTP pathways at 30-40 min, p=0.38 (no virus vs CFLSN CALI -1 min), Wilcoxon signed-rank test. (**C**) CALI of CFL-SN was no longer effective when it was induced 50 min after LTP induction. CALI was induced 50 min after HFS (n=10) or not induced (n=10). Bar graph (right) shows summary in changes in fEPSP slope after 30-40 min CALI. Wilcoxon signed-rank test, p=0.97. (**D**) CALI of CFL-SN did not impact LTD. EPSPs were recorded from slices expressing CFL-SN. CALI was either induced 50 min after low-frequency stimulation (LFS) (1 Hz 900 times) (n=7) or not induced (n=7). Bar graph (right) shows summary in changes in fEPSP slope after 30-40 min CALI. Wilcoxon signed-rank test, p=0.90.

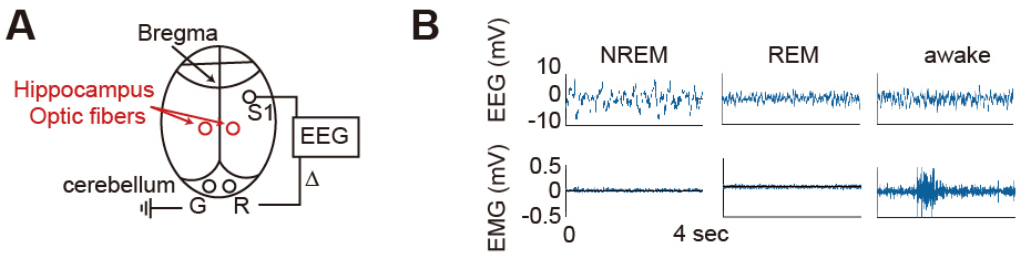

Figure S6. Online analysis of EEG and EMG for sleep state-dependent CALI.
(**A**) Locations of electrodes for EEG recording and optic fibers (red). (**B**) Representative traces of EEG and EMG judged as NREM, REM and awake.

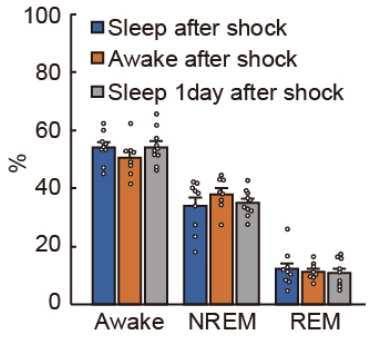

Figure S7. The effect of CALI on sleep states.
Proportion of sleep states (awake, NREM or REM) during 8 h of CALI delivery in three groups of Figure. 3D (CALI during sleep, n=9, CALI during awake, n=8, CALI during sleep 1 day after shock, n=10). CALI did not systemically alter the distributions of behavioral states. p=0.35 (awake), p=0.39 (NREM), p=0.83 (REM), one-way ANOVA respectively.

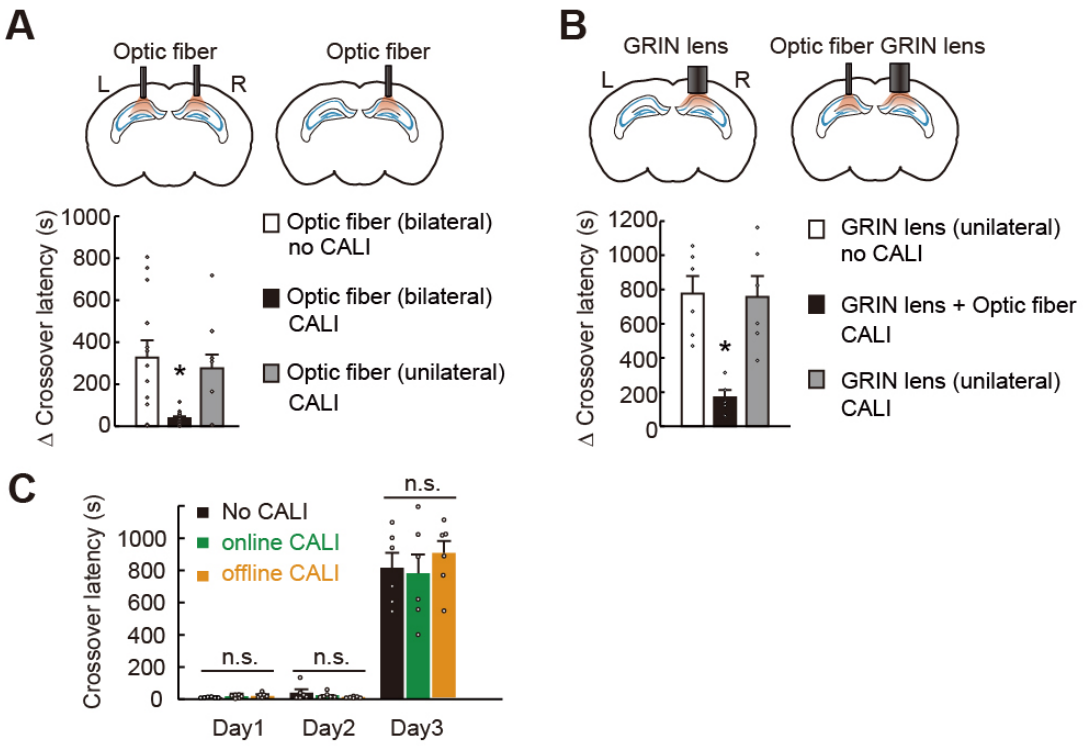

Figure S8. Unilateral CALI had no effect on IA learning.
(**A**) CALI was performed 2 min after shock either bilaterally (same as Figure. 2C) or unilaterally (n=10). One-way ANOVA test followed by Tukey-Kramer post hoc test (versus no CALI). p = 0.0022, F(2,34)=7.34. (**B**) A similar experiment but the illumination of left hemisphere was carried out through GRIN lens used for Ca^{2+}-imaging. n=6 for no CALI; n=5 for bilateral CALI; n=5 for unilateral CALI through GRIN lens. One-way ANOVA test followed by Tukey-Kramer post hoc test (versus no CALI). p = 0.0023, F(2,14)=11.12. (**C**) Averaged crossover latency of no CALI (n=6), online CALI (n=6) and offline CALI (n=6) mice in calcium imaging experiments. Significant difference among 3 groups in each day was not observed. One-way ANOVA test. p=0.12 (Day1), p=0.31 (Day2), p=0.6172.

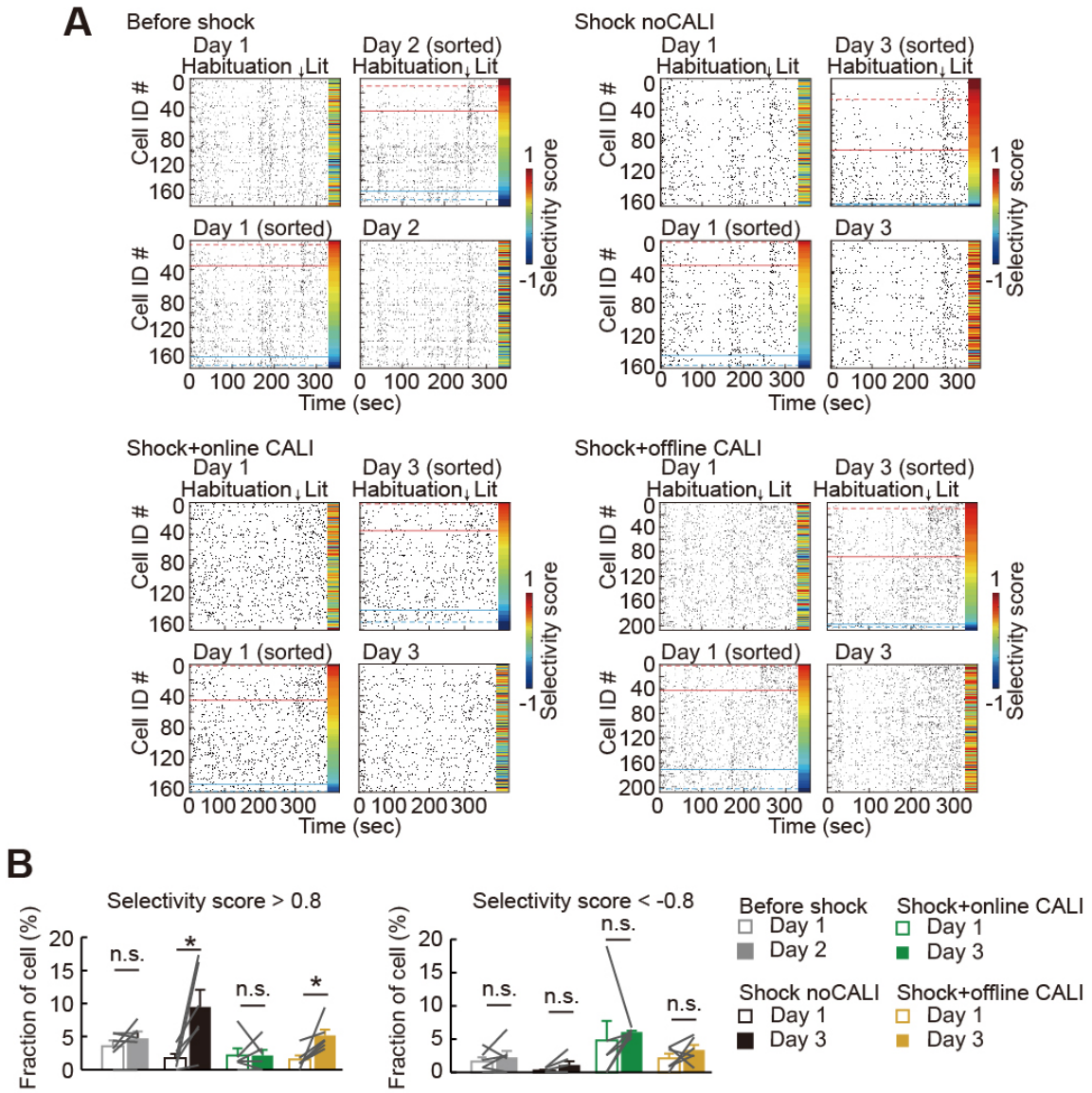

Figure S9. The effect of online and offline LTP erasure on neuronal firing selectivity. (**A**) Example data of Figure. 4C-E. Raster plot of neuronal firing in habituation chamber and IA test chamber. At time position indicated by an arrow, the mice were transferred to the lit side of the IA test chamber. Only cells that can be identified in both Day 1 and Day 3 were plotted. Top and bottom panels show the same set of neurons but sorted by the selectivity index on day 3 and day 1, respectively. Red and blue solid lines indicate selectivity score of 0.4 and -0.4 and dotted lines indicates 0.8 and -0.8. (**B**) Fraction of cells showing selectivity score >0.8 and <-0.8 respectively. All n=6. Paired t-test. Selectivity score>0.8, p= 0.25 (Before Shock), p= 0.036 (Shock no CALI), p= 0.96 (Shock+online CALI), p=0.029 (Shock+offline CALI); Selectivity score < -0.8, p= 0.50 (Before Shock), p= 0.13 (Shock noCALI), p=0.68 (Shock+online CALI), p=0.35 (Shock+offline CALI).

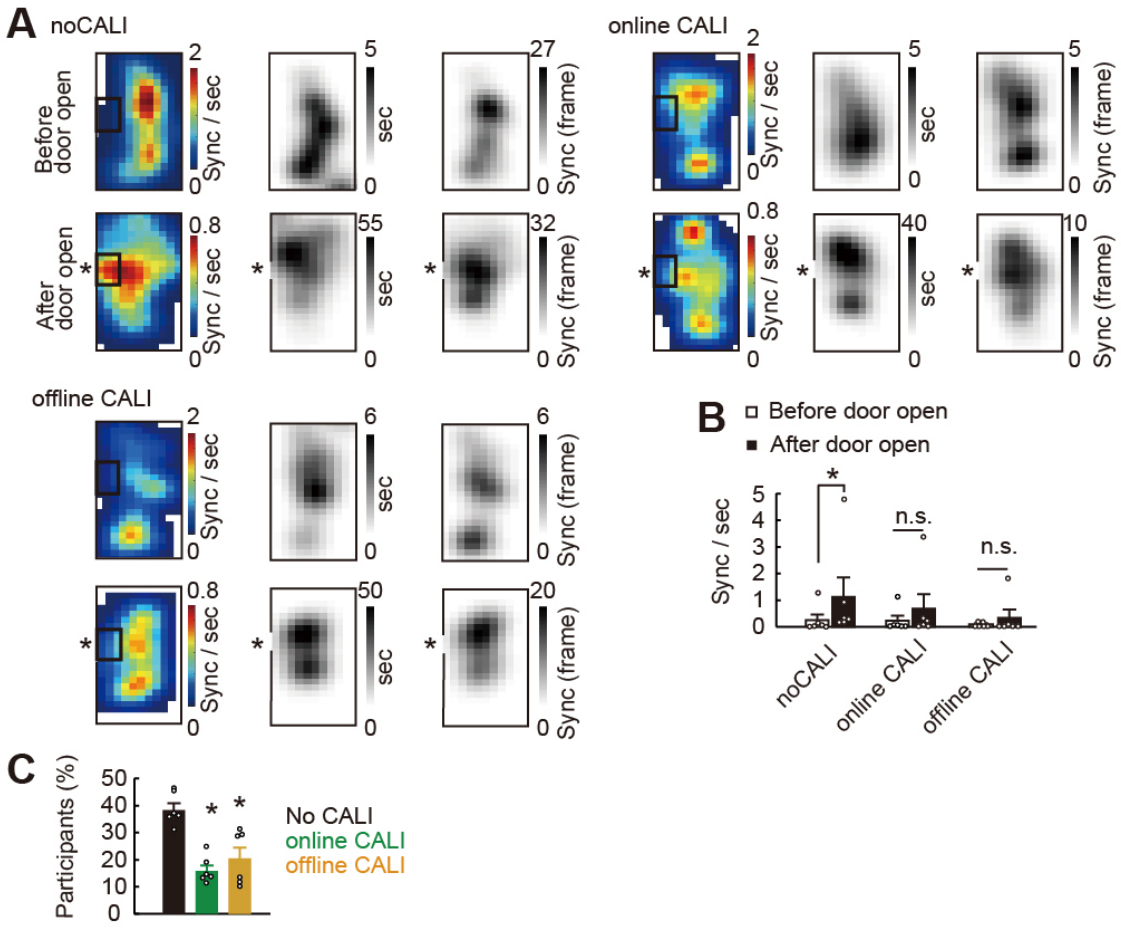

Figure S10. The effect of online and offline LTP erasure on synchronous events.
(**A**) Occupancy time and number of synchronous firing in the lit side of the IA test chamber before and after the door opens. Average of 6 animals from noCALI mice, online CALI mice and offline CALI mice are shown respectively. Raw trajectories of the animals and the position of synchronous firing are shown in Figure 4I. (**B**) Synchronous activity rate averaged from bins (4 cm x 3 cm, rectangle in the heat map) adjacent to the door from each mouse. no CALI, n=6 mice. p=0.04; Online CALI, n=6 mice. p=0.06; Offline CALI, n=6 mice. p=0.80, Wilcoxon signed-rank test. (**C**) Percentage of cells which participate in synchronous events from cells detected in both day 1 and day 3. n=6 mice, each. One-way ANOVA test followed by Tukey-Kramer post hoc test with respect to No CALI, p=0.0002 (online CALI), p=0.0019 (offline CALI), $F_{(2,15)}$=16.06.

References and Notes

1. M. Sakaguchi, Y. Hayashi, Catching the engram: Strategies to examine the memory trace. *Mol. Brain* **5**, 32 (2012). doi:10.1186/1756-6606-5-32 Medline

2. S. Tonegawa, M. D. Morrissey, T. Kitamura, The role of engram cells in the systems consolidation of memory. *Nat. Rev. Neurosci.* **19**, 485–498 (2018). doi:10.1038/s41583-018-0031-2 Medline

3. J. Z. Tsien, P. T. Huerta, S. Tonegawa, The essential role of hippocampal CA1 NMDA receptor-dependent synaptic plasticity in spatial memory. *Cell* **87**, 1327–1338 (1996). doi:10.1016/S0092-8674(00)81827-9 Medline

4. P. W. Frankland, C. O'Brien, M. Ohno, A. Kirkwood, A. J. Silva, α-CaMKII-dependent plasticity in the cortex is required for permanent memory. *Nature* **411**, 309–313 (2001). doi:10.1038/35077089 Medline

5. K. Okamoto, T. Nagai, A. Miyawaki, Y. Hayashi, Rapid and persistent modulation of actin dynamics regulates postsynaptic reorganization underlying bidirectional plasticity. *Nat. Neurosci.* **7**, 1104–1112 (2004). doi:10.1038/nn1311 Medline

6. M. Bosch, J. Castro, T. Saneyoshi, H. Matsuno, M. Sur, Y. Hayashi, Structural and molecular remodeling of dendritic spine substructures during long-term potentiation. *Neuron* **82**, 444–459 (2014). doi:10.1016/j.neuron.2014.03.021 Medline

7. E. Andrianantoandro, T. D. Pollard, Mechanism of actin filament turnover by severing and nucleation at different concentrations of ADF/cofilin. *Mol. Cell* **24**, 13–23 (2006). doi:10.1016/j.molcel.2006.08.006 Medline

8. J. R. Bamburg, A. McGough, S. Ono, Putting a new twist on actin: ADF/cofilins modulate actin dynamics. *Trends Cell Biol.* **9**, 364–370 (1999). doi:10.1016/S0962-8924(99)01619-0 Medline

9. K. Takemoto, T. Matsuda, N. Sakai, D. Fu, M. Noda, S. Uchiyama, I. Kotera, Y. Arai, M. Horiuchi, K. Fukui, T. Ayabe, F. Inagaki, H. Suzuki, T. Nagai, SuperNova, a monomeric photosensitizing fluorescent protein for chromophore-assisted light inactivation. *Sci. Rep.* **3**, 2629 (2013). doi:10.1038/srep02629 Medline

10. K. Kim, G. Lakhanpal, H. E. Lu, M. Khan, A. Suzuki, M. K. Hayashi, R. Narayanan, T. T. Luyben, T. Matsuda, T. Nagai, T. A. Blanpied, Y. Hayashi, K. Okamoto, A Temporary Gating of Actin Remodeling during Synaptic Plasticity Consists of the Interplay between the Kinase and Structural Functions of CaMKII. *Neuron* **87**, 813–826 (2015). doi:10.1016/j.neuron.2015.07.023 Medline

11. E. A. Vitriol, A. L. Wise, M. E. Berginski, J. R. Bamburg, J. Q. Zheng, Instantaneous inactivation of cofilin reveals its function of F-actin disassembly in lamellipodia. *Mol. Biol. Cell* **24**, 2238–2247 (2013). doi:10.1091/mbc.e13-03-0156 Medline

12. N. Honkura, M. Matsuzaki, J. Noguchi, G. C. Ellis-Davies, H. Kasai, The subspine organization of actin fibers regulates the structure and plasticity of dendritic spines. *Neuron* **57**, 719–729 (2008). doi:10.1016/j.neuron.2008.01.013 Medline

13. Q. Zhou, K. J. Homma, M. M. Poo, Shrinkage of dendritic spines associated with long-term depression of hippocampal synapses. *Neuron* **44**, 749–757 (2004). doi:10.1016/j.neuron.2004.11.011 Medline

14. Z. Zhou, J. Hu, M. Passafaro, W. Xie, Z. Jia, GluA2 (GluR2) regulates metabotropic glutamate receptor-dependent long-term depression through N-cadherin-dependent and cofilin-mediated actin reorganization. *J. Neurosci.* **31**, 819–833 (2011). doi:10.1523/JNEUROSCI.3869-10.2011 Medline

15. M. A. Wilson, B. L. McNaughton, Reactivation of hippocampal ensemble memories during sleep. *Science* **265**, 676–679 (1994). doi:10.1126/science.8036517 Medline

16. D. Nakayama, H. Iwata, C. Teshirogi, Y. Ikegaya, N. Matsuki, H. Nomura, Long-delayed expression of the immediate early gene Arc/Arg3.1 refines neuronal circuits to perpetuate fear memory. *J. Neurosci.* **35**, 819–830 (2015). doi:10.1523/JNEUROSCI.2525-14.2015 Medline

17. G. Girardeau, K. Benchenane, S. I. Wiener, G. Buzsáki, M. B. Zugaro, Selective suppression of hippocampal ripples impairs spatial memory. *Nat. Neurosci.* **12**, 1222–1223 (2009). doi:10.1038/nn.2384 Medline

18. L. A. Atherton, D. Dupret, J. R. Mellor, Memory trace replay: The shaping of memory consolidation by neuromodulation. *Trends Neurosci.* **38**, 560–570 (2015). doi:10.1016/j.tins.2015.07.004 Medline

19. Z. Chen, M. A. Wilson, Deciphering Neural Codes of Memory during Sleep. *Trends Neurosci.* **40**, 260–275 (2017). doi:10.1016/j.tins.2017.03.005 Medline

20. K. Ghandour, N. Ohkawa, C. C. A. Fung, H. Asai, Y. Saitoh, T. Takekawa, R. Okubo-Suzuki, S. Soya, H. Nishizono, M. Matsuo, M. Osanai, M. Sato, M. Ohkura, J. Nakai, Y. Hayashi, T. Sakurai, T. Kitamura, T. Fukai, K. Inokuchi, Orchestrated ensemble activities constitute a hippocampal memory engram. *Nat. Commun.* **10**, 2637 (2019). doi:10.1038/s41467-019-10683-2 Medline

21. D. Miyamoto, D. Hirai, C. C. A. Fung, A. Inutsuka, M. Odagawa, T. Suzuki, R. Boehringer, C. Adaikkan, C. Matsubara, N. Matsuki, T. Fukai, T. J. McHugh, A. Yamanaka, M. Murayama, Top-down cortical input during NREM sleep consolidates perceptual memory. *Science* **352**, 1315–1318 (2016). doi:10.1126/science.aaf0902 Medline

22. Y. Ziv, L. D. Burns, E. D. Cocker, E. O. Hamel, K. K. Ghosh, L. J. Kitch, A. El Gamal, M. J. Schnitzer, Long-term dynamics of CA1 hippocampal place codes. *Nat. Neurosci.* **16**, 264–266 (2013). doi:10.1038/nn.3329 Medline

23. P. Rajasethupathy, S. Sankaran, J. H. Marshel, C. K. Kim, E. Ferenczi, S. Y. Lee, A. Berndt, C. Ramakrishnan, A. Jaffe, M. Lo, C. Liston, K. Deisseroth, Projections from neocortex mediate top-down control of memory retrieval. *Nature* **526**, 653–659 (2015). doi:10.1038/nature15389 Medline

24. B. Bontempi, C. Laurent-Demir, C. Destrade, R. Jaffard, Time-dependent reorganization of brain circuitry underlying long-term memory storage. *Nature* **400**, 671–675 (1999). doi:10.1038/23270 Medline

25. P. W. Frankland, B. Bontempi, L. E. Talton, L. Kaczmarek, A. J. Silva, The involvement of the anterior cingulate cortex in remote contextual fear memory. *Science* **304**, 881–883 (2004). doi:10.1126/science.1094804 Medline

26. Y. Zhang, H. Fukushima, S. Kida, Induction and requirement of gene expression in the anterior cingulate cortex and medial prefrontal cortex for the consolidation of inhibitory avoidance memory. *Mol. Brain* **4**, 4 (2011). doi:10.1186/1756-6606-4-4 Medline

27. G. Riedel, J. Micheau, A. G. M. Lam, E. L. Roloff, S. J. Martin, H. Bridge, L. de Hoz, B. Poeschel, J. McCulloch, R. G. M. Morris, Reversible neural inactivation reveals hippocampal participation in several memory processes. *Nat. Neurosci.* **2**, 898–905 (1999). doi:10.1038/13202 Medline

28. E. Shimizu, Y. P. Tang, C. Rampon, J. Z. Tsien, NMDA receptor-dependent synaptic reinforcement as a crucial process for memory consolidation. *Science* **290**, 1170–1174 (2000). doi:10.1126/science.290.5494.1170 Medline

29. A. Hayashi-Takagi, S. Yagishita, M. Nakamura, F. Shirai, Y. I. Wu, A. L. Loshbaugh, B. Kuhlman, K. M. Hahn, H. Kasai, Labelling and optical erasure of synaptic memory traces in the motor cortex. *Nature* **525**, 333–338 (2015). doi:10.1038/nature15257 Medline

30. H. Murakoshi, H. Wang, R. Yasuda, Local, persistent activation of Rho GTPases during plasticity of single dendritic spines. *Nature* **472**, 100–104 (2011). doi:10.1038/nature09823 Medline

31. K. Takemoto, H. Iwanari, H. Tada, K. Suyama, A. Sano, T. Nagai, T. Hamakubo, T. Takahashi, Optical inactivation of synaptic AMPA receptors erases fear memory. *Nat. Biotechnol.* **35**, 38–47 (2017). doi:10.1038/nbt.3710 Medline

32. K. Z. Tanaka, H. He, A. Tomar, K. Niisato, A. J. Y. Huang, T. J. McHugh, The hippocampal engram maps experience but not place. *Science* **361**, 392–397 (2018). doi:10.1126/science.aat5397 Medline

33. T. Kitamura, S. K. Ogawa, D. S. Roy, T. Okuyama, M. D. Morrissey, L. M. Smith, R. L. Redondo, S. Tonegawa, Engrams and circuits crucial for systems consolidation of a memory. *Science* **356**, 73–78 (2017). doi:10.1126/science.aam6808 Medline

34. G. Vetere, L. Restivo, C. J. Cole, P. J. Ross, M. Ammassari-Teule, S. A. Josselyn, P. W. Frankland, Spine growth in the anterior cingulate cortex is necessary for the consolidation of contextual fear memory. *Proc. Natl. Acad. Sci. U.S.A.* **108**, 8456–8460 (2011). doi:10.1073/pnas.1016275108 Medline

35. K. Takehara-Nishiuchi, Prefrontal-hippocampal interaction during the encoding of new memories. *Brain Neurosci. Adv.* **4**, 2398212820925580 (2020). doi:10.1177/2398212820925580 Medline

36. N. Maingret, G. Girardeau, R. Todorova, M. Goutierre, M. Zugaro, Hippocampo-cortical coupling mediates memory consolidation during sleep. *Nat. Neurosci.* **19**, 959–964 (2016). doi:10.1038/nn.4304 Medline

37. F. Xia, B. A. Richards, M. M. Tran, S. A. Josselyn, K. Takehara-Nishiuchi, P. W. Frankland, Parvalbumin-positive interneurons mediate neocortical-hippocampal interactions that are necessary for memory consolidation. *eLife* **6**, e27868 (2017). doi:10.7554/eLife.27868 Medline

38. Y. D. Riani, T. Matsuda, K. Takemoto, T. Nagai, Green monomeric photosensitizing fluorescent protein for photo-inducible protein inactivation and cell ablation. *BMC Biol.* **16**, 50 (2018). doi:10.1186/s12915-018-0514-7 Medline

39. J. C. Grieger, V. W. Choi, R. J. Samulski, Production and characterization of adeno-associated viral vectors. *Nat. Protoc.* **1**, 1412–1428 (2006). doi:10.1038/nprot.2006.207 Medline

40. A. Bota, A. Goto, S. Tsukamoto, A. Schmidt, F. Wolf, A. Luchetti, J. Nakai, H. Hirase, Y. Hayashi, Shared and unique properties of place cells in anterior cingulate cortex and hippocampus. *bioRxiv* 2021.03.29.437441 [Preprint] (2021); doi.org/10.1101/2021.03.29.437441